




Identification of PAX6 and NFAT4 as the Transcriptional Regulators of the Long Noncoding RNA Mrhl in Neuronal Progenitors

Debosree Pal,^{a*} Sangeeta Dutta,^a Dhanur P. Iyer,^{a§} Deepika Shriram,^a Utsa Bhaduri,^a  M. R. S. Rao^a

^aMolecular Biology and Genetics Unit, Jawaharlal Nehru Centre for Advanced Scientific Research, Bangalore, Karnataka, India

Debosree Pal and Sangeeta Dutta contributed equally to this work. Author order was determined in the order of conceptualization and work done.

ABSTRACT The long noncoding RNA (lncRNA) Mrhl has been shown to be involved in coordinating meiotic commitment of mouse spermatogonial progenitors and differentiation events in mouse embryonic stem cells. Here, we characterized the interplay of Mrhl with lineage-specific transcription factors during mouse neuronal lineage development. Our results demonstrate that Mrhl is expressed in the neuronal progenitor populations in mouse embryonic brains and in retinoic acid-derived radial-glia-like neuronal progenitor cells. Depletion of Mrhl leads to early differentiation of neuronal progenitors to a more committed state. A master transcription factor, PAX6, directly binds to the Mrhl promoter at a major site in the distal promoter, located at 2.9 kb upstream of the transcription start site (TSS) of Mrhl. Furthermore, NFAT4 occupies the Mrhl-proximal promoter at two sites, at 437 base pairs (bp) and 143 bp upstream of the TSS. Independent knockdown studies for PAX6 and NFAT4 confirm that they regulate Mrhl expression in neuronal progenitors. We also show that PAX6 and NFAT4 associate with each other in the same chromatin complex. NFAT4 occupies the Mrhl promoter in PAX6-bound chromatin, implying possible coregulation of Mrhl. Our studies are crucial for understanding how lncRNAs are regulated by major lineage-specific transcription factors, in order to define specific development and differentiation events.

KEYWORDS Mrhl, lncRNA, NPCs, transcription factor, brain, PAX6

Noncoding RNA dominates the eukaryotic transcriptome, contributing up to 80 to 90% of it (1). Long noncoding RNAs (lncRNAs) are classified as a major class of noncoding RNAs with a length greater than 200 nucleotides, with no or little translational activity (2, 3). lncRNAs which do show little translational activity have been reported to possess small open reading frames which encode small peptides or micro-peptides of fundamental biological importance (4, 5). Although most lncRNAs are not well conserved, their highly specific spatial-temporal expression has highlighted their complex roles in diverse biological functions during development and differentiation. In addition, their dysregulation has been associated with several diseases, including cancer and neurological disorders (2, 6–10). Several studies have verified the importance of long noncoding RNAs as functional regulators. To regulate their targets, lncRNAs are known to use a wide variety of mechanisms at both transcriptional and posttranscriptional levels (11–14).

During development of a mammalian system, synchronous expression and repression of genes lead to a staggering variety of cells with various functional activities. This remarkable orchestration of genetic components is most evident in an extremely complex system of mammalian neural development and in the brain, with its intricate cellular architecture, maintenance, and function. However, regulators behind this fine coordination are still elusive. With a large number of highly specific lncRNAs expressed

Copyright © 2022 American Society for Microbiology. All Rights Reserved.

Address correspondence to M. R. S. Rao, mrsrao@jncasr.ac.in.

*Present address: Debosree Pal, Blizzard Institute, Barts and the London School of Medicine and Dentistry, Queen Mary University of London, London, United Kingdom.

§Present address: Dhanur P. Iyer, Department for Genome Regulation, Max Planck Institute for Molecular Genetics, Berlin, Germany.

◇Present address: Utsa Bhaduri, Department of Life Sciences, University of Trieste, Trieste, Italy, and European Union's Horizon 2020 TRIM-NET Innovative Training Network (ITN) of Marie Skłodowska Curie Actions (MSCA), University of Trieste, Trieste, Italy.

The authors declare no conflict of interest.

Received 27 January 2022

Returned for modification 2 March 2022

Accepted 30 September 2022

Published 1 November 2022

in the brain, their contribution in neuronal development is undeniable (15–21). Data from the GENCODE v7 catalog suggest that 40% of most differentially expressed lncRNAs are specific for the brain (20). A notable aspect is their distinct neuroanatomical loci, along with developmental and stage-specific expression, as evident in many studies (22–27). For example, Goff et al. used mutant mouse models for 13 lncRNAs and assessed their expression pattern from brains at embryonic day 14.5 (E14.5) to adult brains, revealing high variability in the expression pattern for each lncRNA both spatially and temporally (28). Along with characteristic lncRNA expression signatures in subregions of the brain and specific neuronal populations, studies have also shown lncRNA-mRNA pairs, sharing a genomic locus, to display specific coexpression in a region-specific manner. For example, lncRNA GM9968 and the DNA-binding-protein gene *Zbtb20* show high enrichment in hippocampus (21). Transcriptome analysis by Lv et al. revealed the development stage specificity of lncRNAs in mice (23). They annotated a large number of lncRNAs to the embryonic brain. Interestingly, they found that expression of a majority of them was very low or nonevident in the adult brain, suggesting their significance during embryonic brain development (23).

lncRNAs have been shown to undergo regulated expression during development and differentiation (29). Studies have verified dynamic expression and regulation of many lncRNAs in conjunction with stage-specific transcription factors (TFs) during *in vitro* differentiation scenarios, like that of mouse embryonic stem (mES) cells to embryoid bodies (EBs) or during retinoic acid-mediated neuronal differentiation of ES cells (24, 25). Observations from these studies indicate association of pluripotent TFs like SOX2, OCT4, and NANOG at the promoter of lncRNAs, modulating their expression during development. For example, the lncRNA [AK028326](#) (Gomafu; synonym: Miat) is activated by OCT4, while the lncRNA [AK141205](#) is repressed by NANOG, resulting in the modulation of mES cell pluripotency (26). This tightly controlled differential expression pattern of lncRNAs is thus important for the delicate balance between lineage commitment and maintenance of pluripotent status. Loss- and gain-of-function studies for lncRNAs have shown that they act to regulate TFs as well, causing deregulation of lineage specification. For example, in a study by Zhang et al., inducible knockdown of the lncRNAs Rik-201 and Rik-203 in mES cells led to inhibition of neural differentiation by modulating the expression of SOX6 (30). A separate study identified lncRNA Sox2OT as a promoting factor for cortical neural progenitors by repressing the expression of the pluripotent gene *Sox2* via physical interaction with the multifunctional transcriptional regulator YY1 (31). The lncRNA Rmst has been shown to physically interact with SOX2 to alter the fate of neural stem cells (32).

The lncRNA Mrhl (meiotic recombination hot spot locus; also known as Hm629797), an lncRNA that has been studied extensively by our group, was the focus of our present study (14, 33–38). Mrhl is an intronic and single-exonic lncRNA with a length of 2.4 kb. This nucleus-restricted lncRNA is transcribed from the 15th intron of *Phkb* in mice and shows syntenic conservation in humans (34, 39, 40). Mrhl is found to be a negative regulator of WNT signaling via its interaction with p68/DDX5 RNA helicase in mouse spermatogonial cells (34, 35, 37). lncRNA Mrhl has also been shown to regulate *Sox8* at chromatin level signifying its role in meiotic commitment of mouse spermatogonial progenitor cells (36). Our latest findings from transcriptomics and genome-wide occupancy studies of Mrhl in mouse ES cells revealed its role as a chromatin regulator of cellular differentiation and development genes (38).

Taking clues from our recent study (38), in which a large number of genes related to neural development and differentiation were dysregulated upon Mrhl downregulation, in the present study we explored the dynamic expression pattern of lncRNA Mrhl and its transcriptional regulation during mouse neuronal lineage development. We have shown that Mrhl is predominantly expressed in the neuronal progenitor populations in the ventricular-subventricular zones of developing mouse embryonic brains. We have adopted an *in vitro* model system of retinoic acid-mediated derivation of radial-glia-like neuronal progenitor cells (NPCs) from mES cells. Mrhl shows upregulation

of expression in these NPCs. The level of lncRNA Mrhl is significantly downregulated in postnatal brains and in maturing neurons, suggesting its significance in embryonic neuronal lineage development. Further studies revealed that NPCs undergo premature commitment to neurons when Mrhl is depleted, implying its importance in neuronal fate specification.

We have also identified PAX6, a master transcription factor in NPCs, as a regulator of Mrhl transcription. Further exploration of this mechanism revealed that PAX6 plays this role by physically binding to the promoter of Mrhl at multiple sites of action. A major site of action for PAX6 on the Mrhl promoter is situated 2.9 kb upstream of the transcription start site (TSS), where it binds directly and regulates Mrhl in NPCs. Three other minor sites are present at 1.27 kb, 672 base pairs (bp), and 622 bp upstream of the TSS of Mrhl, where regulation is proposed to be carried out by PAX6 and/or its isoform PAX6(5A) and potentially in conjunction with other cofactors. NFAT4, which is another important transcription factor in neuronal development, was also found to be enriched at the promoter region of Mrhl at two sites in the proximal promoter, 437 bp and 143 bp upstream of the TSS. Knockdown of PAX6 or NFAT4 led to downregulation of Mrhl transcript levels in NPCs, confirming regulation. Chromatin immunoprecipitation (ChIP) followed by Western blotting revealed that PAX6 and NFAT4 associate with each other, whereas sequential ChIP showed that NFAT4 binds to the Mrhl promoter in PAX6-bound chromatin, suggesting that PAX6 might regulate Mrhl together with NFAT4 in NPCs. This study thus reveals that regulated expression of the lncRNA Mrhl by multiple and specific TFs during neuronal lineage development is important for determining cell fate.

RESULTS

Mrhl is predominantly expressed in embryonic stages of the mouse brain and in the neuronal progenitor population. Our recent study on the transcriptome analysis of mES cells following downregulation of Mrhl lncRNA showed an overrepresentation of neuronal lineage-specific genes and networks to be dysregulated (38). Based on this observation, we initiated this study to address the role of Mrhl in neuronal lineage specification. To begin with, we analyzed its expression level in the mouse brain tissues of both embryonic and postnatal mice. We performed quantitative reverse transcription-PCR (qRT-PCR) on brains from E10.5 to E18.5 and postnatal stages P0 to P40 and observed that Mrhl expression is predominantly abundant at E12.5 to E18.5 (Fig. 1A). Furthermore, Mrhl showed abrupt decrease in expression level from postnatal stage P0 onward.

At around E8 of brain development, neuroepithelial cells of the neural tube give rise to radial glial cells (RGCs), the future NPCs of the brain. RGCs undergo rapid proliferation and specification into basal progenitors, which in turn give rise to neurons, with a peak of neurogenesis at E14 (41). Since we observed the first peak of Mrhl expression at E14.5 in our studies, we focused on understanding its role at this stage. We isolated brain tissue from E14.5 embryos and divided them into fore-, mid- and hindbrain regions based on their gross anatomy. We confirmed the purity of the three regions obtained based on the forebrain-specific marker FoxG1, the midbrain-specific marker En1, and the hindbrain-specific marker Gbx2 (42, 43). PAX6 was used a control marker owing to its defined expression pattern across the three regions of the brain.

We observed that Mrhl is expressed ubiquitously across all the three regions of the mouse brain at E14.5 (Fig. 1B). While Mrhl may have specific roles to play across all regions of the developing brain, we concentrated on the forebrain development. To further narrow down the specific cell types in which Mrhl might be involved in the forebrain, we performed RNA fluorescence *in situ* hybridization (FISH) for Mrhl, along with immunofluorescence (IF) assays for PAX6 as the marker, on whole forebrain sections at E14.5. We found that Mrhl is expressed specifically in the ventricular/subventricular zone of the brain at this stage (Fig. 1C). This was further confirmed by analyzing publicly available ChIP sequencing (ChIP-Seq) data sets (accession no. [GSE93009](#)) for RNA polymerase II (Pol II), RNA Pol II-Ser5p (initiation polymerase), the transcription

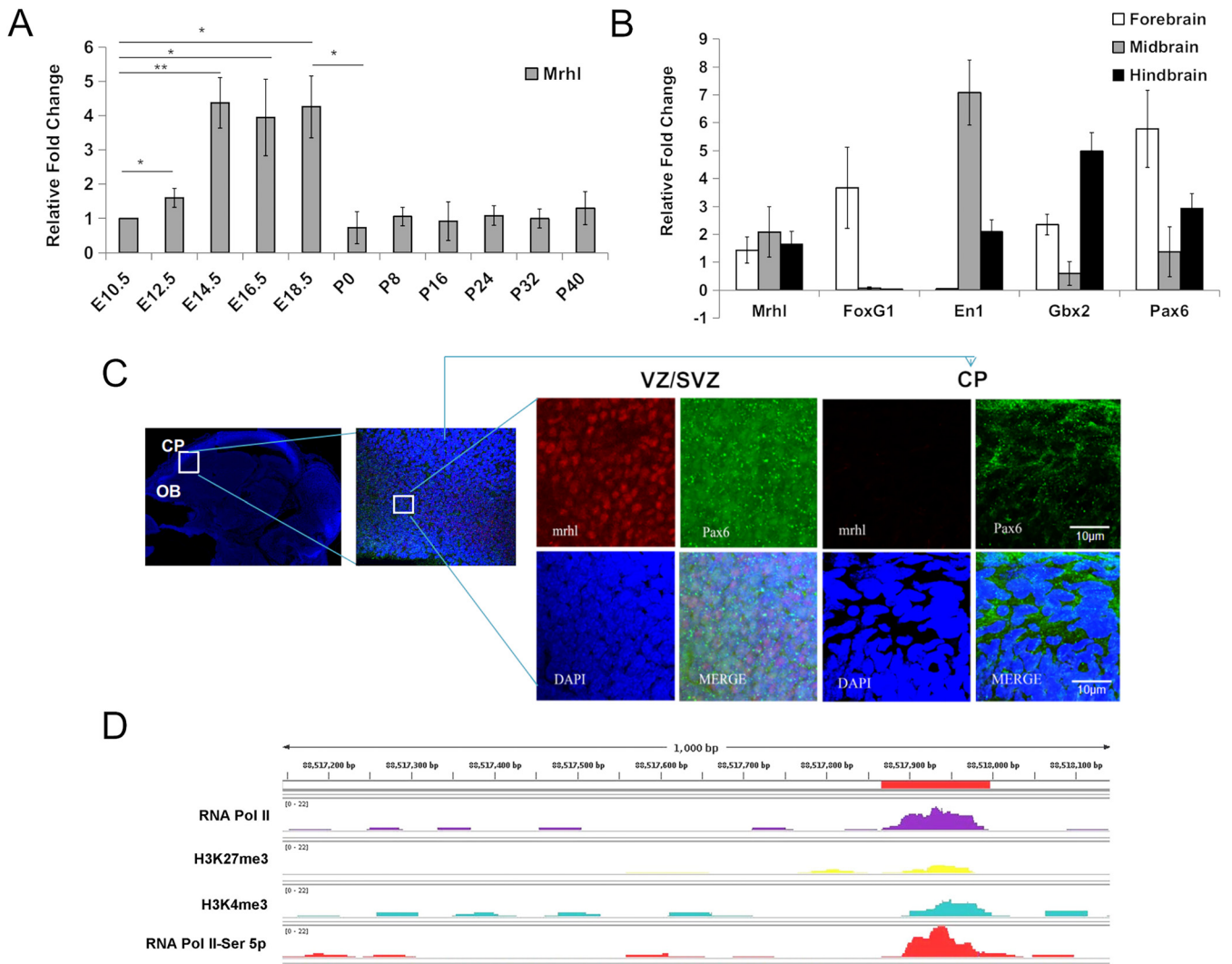


FIG 1 Mrhl is predominantly expressed in the neuronal progenitor population of the developing mouse embryonic brain. (A) qPCR data for Mrhl expression in embryonic and postnatal mouse brains showed abundance at E12.5 to E18.5. (B) qPCR for Mrhl expression across different regions of the E14.5 brain along with region-specific markers revealed a ubiquitous expression pattern of Mrhl. (C) RNA FISH for Mrhl and IF for PAX6 in E14.5 brain sections showed predominant expression of Mrhl in ventricular-subventricular (VZ/SVZ) zones of the brain concomitant with PAX6 nuclear expression. CP, cortical plate; OB, olfactory bulb. (D) Analysis of available ChIP-Seq data sets for enrichment of RNA Pol II or histone modifications on the Mrhl 1-kb promoter in Nestin-positive cells from E15.5 cortices. Error bars indicate standard deviations (SD) from three independent experiments, with replicates in each ($n = 6$ to 20). *, $P < 0.05$; **, $P < 0.01$; ***, $P < 0.001$ (Student's t test). Bar = $10 \mu\text{m}$.

activation mark H3K4me3, and the transcription repression mark H3K27me3 on the proximal 1-kb promoter of Mrhl in Nestin-positive NPCs isolated from E15.5 cortices (44). The analysis showed distinct enrichments for RNA Pol II, initiating RNA Pol II and H3K4me3 near the TSS for Mrhl (Fig. 1D). Thus, we concluded that Mrhl is predominantly expressed in the neuronal progenitor population of the developing embryonic mouse brain.

Mrhl expression pattern in mouse brain is recapitulated in an *in vitro* differentiation model. We adopted the well-established retinoic acid (RA)-induced *in vitro* differentiation model system to further elucidate Mrhl as a molecular player in NPCs. We generated EBs from mouse ES cells and treated them with RA by the 4-/-4+ method (Fig. 2A). This method has been shown to generate PAX6+ RGC-like NPCs that possess the capability to generate neurons *in vivo*, as shown by the studies by Bibel et al. (45) and Plachta et al. (46). We observed that Mrhl expression is upregulated in RA-treated EBs compared to vehicle-treated EBs (Fig. 2B). An analysis for various NPC markers such as PAX6 and Nestin as well as neuronal markers such Tuj1 (beta-III tubulin) and Ascl1

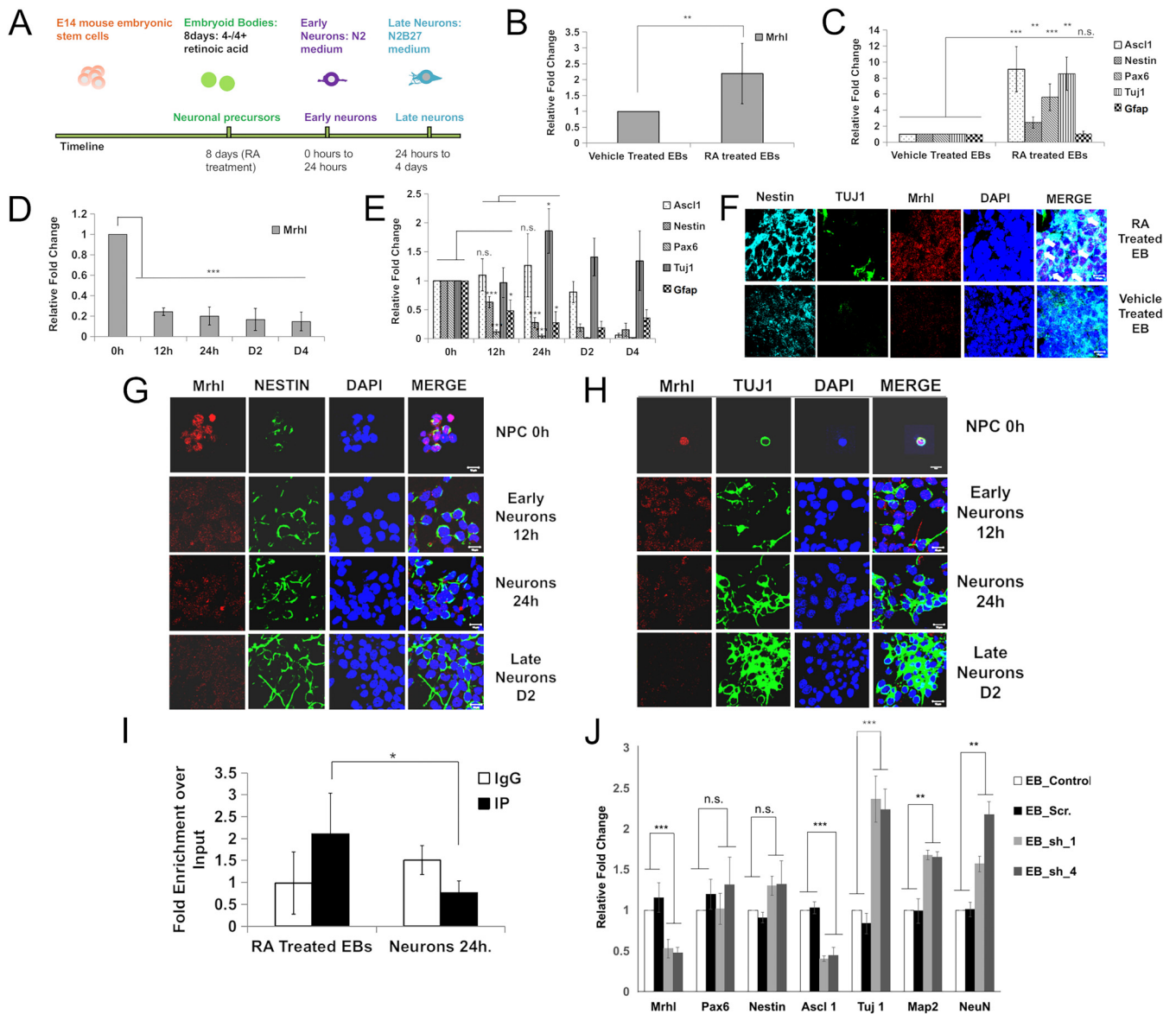


FIG 2 Mrhl expression in embryonic brain is recapitulated in an *in vitro* model. (A) Schematic representing the model system in our study. (B) qPCR analysis of Mrhl expression in RA- versus vehicle-treated EBs showed distinctly higher expression in RA-treated EBs. (C) qPCR analysis of various markers for neuronal lineage in RA-treated versus vehicle-treated EBs. Ascl1 is a neuronal lineage marker. Nestin and PAX6 are NPC markers. Tuj1 is a maturing neuron marker. Gfap is an astrocyte lineage marker. (D) qPCR analysis of Mrhl expression in 12 h to D4 maturing neurons showed downregulation of Mrhl levels in neurons. (E) qPCR analysis of various markers for NPCs and neurons at different hours of differentiation showed reduction in NPC markers and an increase in neuron marker. (F) RNA FISH for Mrhl and IF for the NPC marker Nestin and the maturing neuron marker Tuj1 in EB sections confirming the above observations. White arrows indicate localization of Mrhl. (G and H) RNA FISH for Mrhl followed by IF for Nestin and Tuj1 in neurons to validate above qPCR data. (I) ChIP-qPCR for H3K4me3 on the proximal Mrhl promoter in RA-treated EBs versus neurons at 24 h is in agreement with higher Mrhl expression in NPCs. (J) qPCR analysis for NPC and neuron markers in Mrhl control versus shRNA EBs showed premature commitment of NPCs to neurons upon Mrhl depletion. Error bars indicate SD from three independent experiments, with technical duplicates in each ($n = 6$). *, $P < 0.05$; **, $P < 0.01$; ***, $P < 0.001$ (Student's *t* test). Bar = 10 μm .

confirmed our *in vitro* neuronal-lineage differentiation system (Fig. 2C and E). We next differentiated these *in vitro*-derived neuronal progenitors into neurons and observed that Mrhl expression is abruptly downregulated from 12 h after neuron formation (Fig. 2D). We further confirmed our observations through RNA FISH for Mrhl and IF for Nestin on cryosections of RA- versus vehicle-treated EBs. RA-treated EB sections showed noticeable expression of Mrhl compared to vehicle-treated sections (Fig. 2F). Similarly, Mrhl showed significant reduction in expression from the early neuron stage at 12 h (Fig. 2G and H). We also performed ChIP-qPCR on RA-treated EBs and neurons at 24 h of differentiation for H3K4me3, an active transcription mark, and the results

indicated a decreased association of this histone mark at the Mrhl promoter in maturing neurons (Fig. 2I). Our observations thus confirm that Mrhl is preferentially expressed in NPCs. We further observed that Mrhl appears to be a low-abundance lncRNA in NPCs, as also observed in our earlier studies in mES cells (38), owing to up-regulation levels of only 2-fold or lower H3K4me3 levels at its promoter.

Mrhl depletion leads to early differentiation of NPCs to neurons *in vitro*. We next wanted to understand the significance of Mrhl expression in the NPC population. For this purpose, we subjected stable Mrhl knockdown mES cell lines to RA-mediated neuronal differentiation. We used two independent short hairpin RNA (shRNA) lines for Mrhl, i.e., sh_1 and sh_4. We observed no major changes in NPC markers such as Pax6 or Nestin (Fig. 2J). However, we observed $\geq 50\%$ reduction in the expression of Ascl1. Ascl1 is known to be an inducer of neuronal differentiation, but in a study by Castro et al. (47), Ascl1 was shown to have a novel role in the specification of neural progenitors and cell proliferation. In our studies, we observed an increase in Ascl1 at the NPC stage in RA-treated EBs (Fig. 2C) and then maintenance of its expression up to at least 24 h of neuron formation (Fig. 2E). We also observed ~ 1.5 - to 2.5-fold increases in the levels of expression of the neuronal markers Tuj1, Map2, and NeuN (Fig. 2J). These results show that depletion of Mrhl leads to premature differentiation of NPCs to neurons, suggesting its importance in cell fate regulation during neuronal lineage development. The evidence also aligns with our observations that Mrhl is downregulated in maturing neurons and postnatal brains. This further implies that Mrhl downregulation is important for the commitment of NPCs to neurons.

A master transcription factor PAX6 was identified as a regulator of Mrhl in NPCs. Next, we were interested in understanding how the transcriptional activity of Mrhl is regulated in neuronal progenitors. lncRNAs act in close coordination with TFs not only to regulate target genes but also to be regulated themselves. The lncRNA Rmst, also known as Ncrms, has been shown to be positively regulated by PAX2, a TF involved in midbrain and cerebellum development (48), whereas it is negatively regulated by REST during neurogenesis (32), emphasizing the context-dependent transcriptional regulation of lncRNAs by major TFs. STAT3 has been shown to upregulate the expression of lncRNA Hoxd-As1 at the transcription level, contributing to invasion and metastasis in hepatocellular carcinoma (49). During male germ cell meiotic commitment, Mrhl is transcriptionally repressed by the WNT signaling pathway effector TCF4/ β -catenin complex, along with the corepressor CTBP1, via interaction at its promoter (37).

We used a combination of the GPMiner (50) and JASPAR (51) programs to gain insights into the probable transcriptional regulators of Mrhl in neuronal progenitors. An analysis of the region 3 kb upstream of the TSS of Mrhl revealed predicted binding sites for diverse lineage-specific TFs (Fig. 3A). With respect to the neuronal lineage, TCF4 (172 bp), PAX6 (2,904 bp, 1,276 bp, 672 bp, and 622 bp), RBPJ-K (484 bp), NFAT (437 bp and 143 bp), and Meis1 (477 bp) were of noticeable importance (Fig. 3A). Initially, we focused on TCF4, an effector of the WNT pathway, owing to our earlier studies on WNT-mediated regulation of Mrhl in B-type spermatogonial progenitors. Additionally, the WNT pathway has been shown to be involved in context-dependent roles in neural development (52–54). Toward this end, we performed IF for β -CATENIN on RA-treated versus vehicle-treated EBs as well as during neuronal differentiation over a period of 2 to 24 h (Fig. 3B). We observed no translocation of β -CATENIN from the membrane to the nucleus, a hallmark of non-activation of the WNT pathway. Hence, we ruled out TCF4 as a potential transcriptional regulator for Mrhl in RA-derived NPCs.

Our studies also suggest that WNT signaling may not have a role to play in RA-derived NPCs. We additionally investigated RBPJ-K, an effector of the NOTCH pathway, since NOTCH signaling has been extensively implicated in the proliferation and maintenance of radial glia progenitors in the brain (55–58). We performed IF for NICD in vehicle-treated versus RA-treated EBs and observed translocation of NICD to the nuclei of RA-derived NPCs (Fig. 3C), indicating activation of the NOTCH pathway. However, subjecting RA-treated EBs to the NOTCH pathway inhibitor DAPT {*N*-[*N*-(3,5-difluorophenacetyl)-*L*-alanyl]-5-phenylglycine *t*-butyl ester} showed a reduction in expression for the

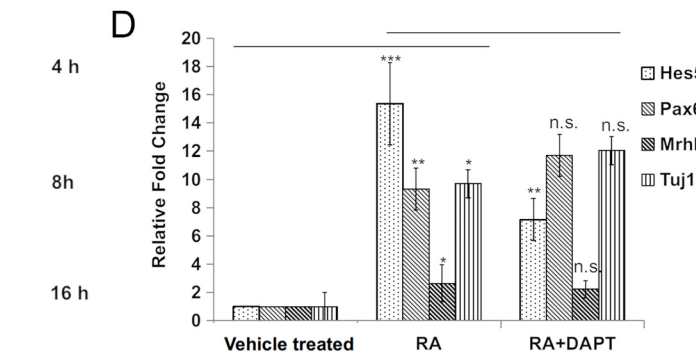
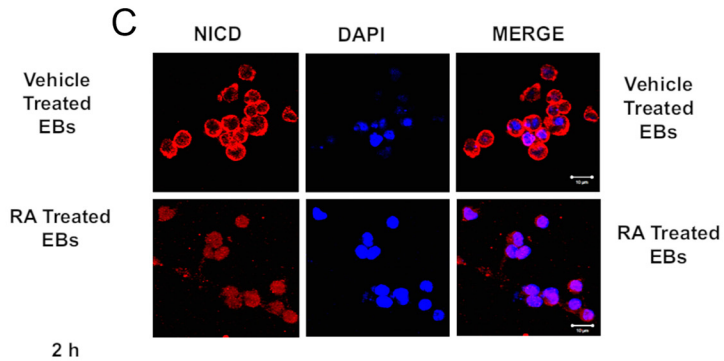
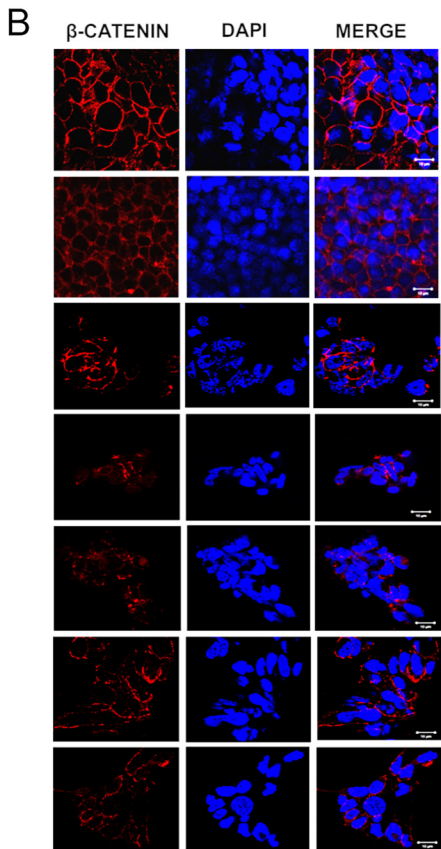
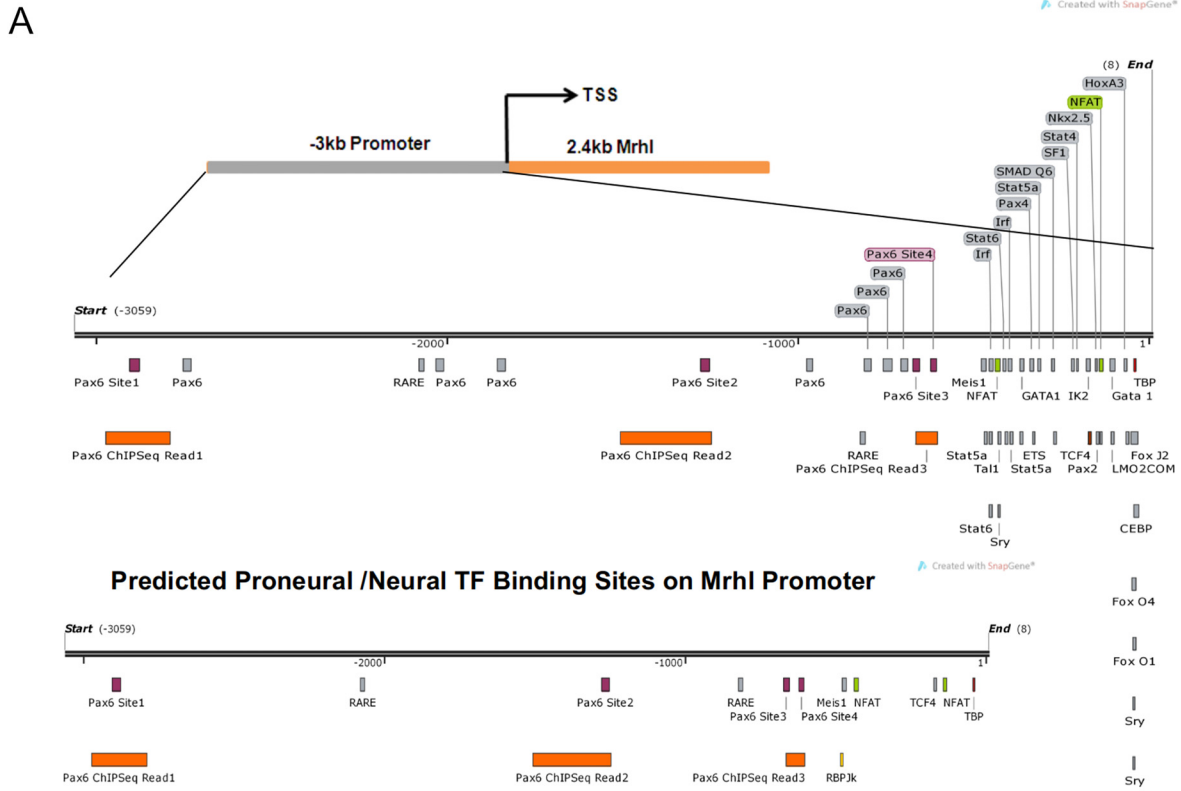


FIG 3 Identification of potential transcriptional regulators for Mrhl during neuronal lineage development. (A) GPMiner and JASPAR analysis for predicted TF binding sites on the Mrhl 3-kb promoter region (created by SnapGene). (B) IF for β -catenin in RA-treated (Continued on next page)

known target Hes5 but not for Mrhl (Fig. 3D), thereby ruling out RBPJ-K as the potential regulator for Mrhl. We also did not see changes in expression levels for other neuronal markers, such as Pax6 and Tuj1, suggesting that in RA-derived NPCs, NOTCH signaling may act through other pathways altogether to regulate progenitor physiology.

We then focused on PAX6, whose role in neural development with respect to NPC specification and neurogenesis has been well established (59, 60). We collected ChIP-Seq data sets available for PAX6 in E12.5 mouse embryonic forebrain (GEO accession number [GSE66961](#)) (61) and combined them with a FIMO analysis for PAX6 motifs (62, 63). We identified four binding sites on the promoter of Mrhl as candidates for PAX6-mediated regulation (Fig. 4A; Table 1, sites 1, 2, 3 and 4). Elaborate studies by Xie and Cvekl (62) have shown that PAX6 binds to nine novel motifs, only one of which corresponds to the consensus. FIMO analysis further revealed the presence of motifs 1-1 and 2-1 in site 1, motifs 1-3 and 3-3 in site 2, and motif 4-1 in sites 3 and 4 (Fig. 4B to D; Table 1). ChIP-qPCR for PAX6 corresponding to sites 1 to 4 on Mrhl promoter showed that PAX6 occupies all sites in E14.5 brains and sites 1, 3, and 4 in RA-treated EBs (Fig. 4E to G). We concluded that PAX6 potentially regulates Mrhl at the transcriptional level in NPCs.

PAX6 physically binds to the distal promoter and regulates Mrhl in NPCs. We next performed an in-depth analysis involving electrophoretic mobility shift assays (EMSA) and luciferase and knockdown assays to understand the regulation of Mrhl by PAX6 at these four sites. We expressed and purified full-length PAX6 and its isoform PAX6(5A) (Fig. 5A) for our EMSA experiments (Table 1). We observed that PAX6 binds directly to site 1 on Mrhl promoter strongly and to site 2 weakly and does not bind to sites 3 and 4 (Fig. 5B). In the studies by Xie and Cvekl (62), it was shown that PAX6 and PAX6(5A) bind to their diverse motifs with various affinities depending on the biological context. Since we observed occupancy of PAX6 in our ChIP results on sites 2, 3, and 4 and since it has already been demonstrated that motif 1-3 in site 2 and motif 4-1 in sites 3 and 4 are bound by PAX6(5A) with moderately high affinity (62), we hypothesized that sites 2, 3 and 4 might be bound by the isoform PAX6(5A). PAX6(5A) differs from PAX6 in that it has a 14-amino-acid insertion in the PAI domain, leading to its differential binding to the various motifs. Furthermore, studies have shown that the ratio of PAX6:PAX6(5A) shifts from 8:1 to 3:1 from E12.5 to E14.5 (64). However, our EMSA studies showed no binding for PAX6(5A) to any of these sites (Fig. 5C).

We then carried out luciferase assays in P19EC cells, which lack expression of endogenous PAX6, using various constructs of the Mrhl promoter harboring one site or the other (Fig. 5D to F) in the presence of ectopically expressed PAX6 or PAX6(5A). Sites 3 and 4 did not elicit any luciferase activity. However, both sites 2 and 1 displayed luciferase activity in the presence of either isoform with an induction of ~ 1.4 -fold. Furthermore, luciferase assays in the presence of both the isoforms revealed the highest activity at a ratio of 4:1 for PAX6 to PAX6(5A) for the Mrhl promoter, causing an induction of ~ 2 -fold (Fig. 5G). Considering that Mrhl is a low-abundance transcript in NPCs, this level of induction of Mrhl might be significant for the cells. Furthermore, it is quite possible that PAX6 needs to interact with another transcription factor binding to the proximal promoter of Mrhl to coregulate the transcription of Mrhl in NPCs. It has been shown that other TFs, such as SOX2, act in conjunction with PAX6 to regulate target genes (60, 65). Finally, we generated doxycycline-inducible PAX6 knockdown mES cell lines and induced the knockdown of PAX6 at day 5 of RA-mediated differentiation of EBs, which was scored for Mrhl expression. We observed a reduction in Mrhl expression concomitant with reduction of PAX6 expression (Fig. 5H). From these studies, we infer that PAX6 transcriptionally regulates Mrhl in neuronal progenitors through direct

FIG 3 Legend (Continued)

versus vehicle-treated EBs and different time points of neuronal differentiation showed lack of involvement of the WNT pathway in this model system. (C) IF for NICD in RA versus vehicle-treated EBs showed activation of the NOTCH pathway. (D) qPCR analysis for genes upon DAPT treatment revealed that NOTCH does not regulate Mrhl in NPCs. Error bars indicate SD from three independent experiments, with technical duplicates in each ($n = 6$). *, $P < 0.05$; **, $P < 0.01$; ***, $P < 0.001$ (Student's t test). Bar = 10 μm .

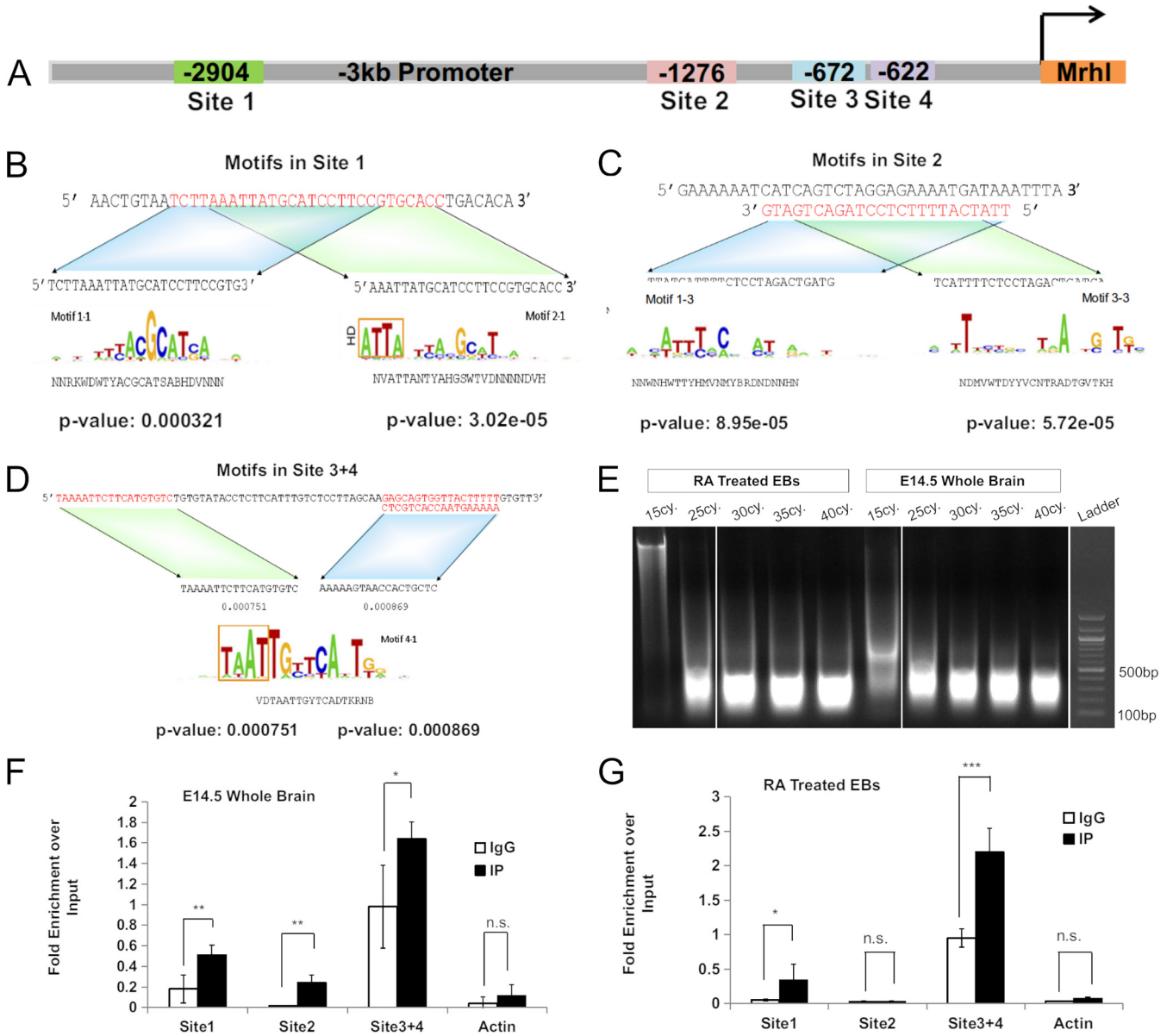


FIG 4 Identification of PAX6 as the transcriptional regulator of Mrhl in NPCs. (A) Schematic showing PAX6 binding sites on the 3-kb promoter of Mrhl as analyzed from publicly available ChIP-Seq data and FIMO analysis. (B to D) Motifs for PAX6 on Mrhl promoter sites 1 to 4 as revealed by FIMO analysis. (E) Sonication pattern for chromatin isolated from RA-treated EBs and E14.5 whole brain. Sonication efficiency was initially checked for a smaller number of cycles (15 and 25) before proceeding to a higher number of cycles to get the desired enrichment between 200 and 500 bp. (F and G) ChIP-qPCR analysis for PAX6 enrichment on the Mrhl promoter in E14.5 whole brain and RA-treated EBs, respectively. Error bars indicate SD from three independent experiments, with technical duplicates in each ($n = 6$). *, $P < 0.05$; **, $P < 0.01$; ***, $P < 0.001$ (Student's t test).

physical binding at site 1 on the distal promoter of Mrhl. Site 2 may also be a point of regulation by PAX6/PAX6(5A), as is evidenced by our ChIP and luciferase assays, probably in conjunction with other TFs/cofactors. Sites 3 and 4 showed enrichment for PAX6 in our ChIP assays but no binding or activity in our EMSAs and luciferase assays, suggesting that regulation via these two sites might be highly context dependent.

Regulation of Mrhl by NFAT4 in NPCs at the proximal promoter. The experiments described above clearly demonstrate that PAX6 regulates Mrhl expression in NPCs, primarily through upstream distal site 1 at 2.9 kb in the promoter of Mrhl. Since this site is located far upstream of the promoter of Mrhl, we argued that there must be other TFs that act to regulate Mrhl via its core proximal promoter and that they may act in conjunction with PAX6. As mentioned earlier, SOX2 along with PAX6 has been shown to coregulate target genes during neuronal or lens development (60, 65). From

TABLE 1 PAX6 binding sites and corresponding EMSA probes used for the Mrhl promoter, 3 kb upstream from the TSS

Position (mm9 genome, chromosome 8)	Strand	Motif	Matched sequence	P	EMSA probe	Site (position [bp])
88515239–88515262	+	1-1	TCTTAAATTATGCATCCTTCCGTG	0.000321	1	1 (2904)
88515243–88515266	+	2-1	AAATTATGCATCCTTCCGTGACC	3.02e–05	1	1 (2904)
88516867–88516890	–	1-3	TTATCATTTTCTCCTAGACTGATG	8.95e–05	2	2 (1276)
88516869–88516887	–	3-3	TCATTTTCTCCTAGACTGATGA	5.72e–05	2	2 (1276)
88517471–88517489	+	4-1	TAAAATTCTTCATGTGTC	0.000751	3	3 (672)
88517521–88517438	–	4-1	AAAAAGTAACCACTGCTC	0.000869	4	4 (622)

our earlier analysis of the 3-kb region upstream of the TSS for Mrhl (Fig. 3A), we observed that NFAT, TCF4, RBPJ-K, and Meis1 have potential binding sites in the proximal promoter of Mrhl. We had already shown that WNT and NOTCH pathways are not involved in regulating Mrhl in RA derived NPCs (Fig. 3B); therefore, we focused on NFAT and MEIS1.

MEIS1 has been implicated in innervation in the neural crest (66) during RA-mediated neural differentiation of mouse P19EC cells (67) and in granule cells during development of the cerebellum (68). NFAT has been implicated in various aspects of neural development, such as axon growth, neuronal survival, and synapse communication (69, 70). NFAT showed two possible binding sites at 143 bp (BS 1) and 437 bp (BS 2) upstream from the Mrhl TSS, while the MEIS1 binding site was found at 477 bp upstream. Since NFAT has four isoforms, all of which are involved in neural pathways, we first established which isoform of NFAT could regulate Mrhl in NPCs through PCR studies. We observed by semiquantitative PCR that only the isoform NFAT4 is expressed in both E14.5 embryonic brains and EBs (Fig. 6A and B). We further confirmed this by qPCR and observed that, indeed, NFAT4 exhibits the highest expression among all isoforms in embryonic brains (expression was compared with that in P4 brain in each case) (Fig. 6C). We next performed ChIP-qPCR to verify the enrichment of both NFAT4 and MEIS1 at the promoter of Mrhl. Our results show highly significant enrichment of NFAT4 at both the predicted binding sites (Fig. 6D). Although MEIS1 also showed significant enrichment at the Mrhl promoter, the enrichment was ~4-fold lower than that with NFAT4. Therefore, we focused on NFAT4.

We generated an mES cell stable inducible knockdown line for NFAT4 and observed that upon doxycycline-mediated induction of NFAT4 knockdown, Mrhl levels were also significantly reduced, confirming that NFAT4 regulates Mrhl (Fig. 6E). Next, we tried to determine if NFAT4 associates with PAX6 for possible coregulation of Mrhl. First, we performed ChIP followed by Western blotting (ChIP-WB) which clearly demonstrated enrichment of PAX6 during NFAT4-IP and vice versa (Fig. 6F), suggesting the co-occurrence of PAX6 and NFAT4 in the same chromatin complex in RA-derived NPCs. Then, we performed a sequential ChIP assay wherein we pulled down PAX6 chromatin-bound sites in the genome and then carried out NFAT4 ChIP. We observed more than 2-fold enrichment for NFAT4 at Mrhl BS 2 in the sequential ChIP relative to the single ChIP assay (Fig. 6G). This experiment conclusively proved that NFAT4 that coprecipitates with PAX6 is indeed bound to the Mrhl promoter. Findings from these results led us to the conclusion that PAX6 regulates Mrhl at the distal promoter whereas NFAT4 acts to regulate Mrhl at the proximal promoter in NPCs. There is a further possibility that PAX6 and NFAT4 act together to regulate lncRNA Mrhl in NPCs in order to regulate cell fate decisions (Fig. 6H).

DISCUSSION

The role of lncRNAs in development, differentiation, regulation of lineage specification, and maintenance of pluripotency is well established, with numerous examples reported in the literature. Using high-throughput technologies, a large number of lncRNAs have been found to be expressed during neural development and in the brain (10, 15–25). Owing to their specificity and their tight spatial and temporal regulation of expression and functions, lncRNAs have been shown to be more potent indicators of

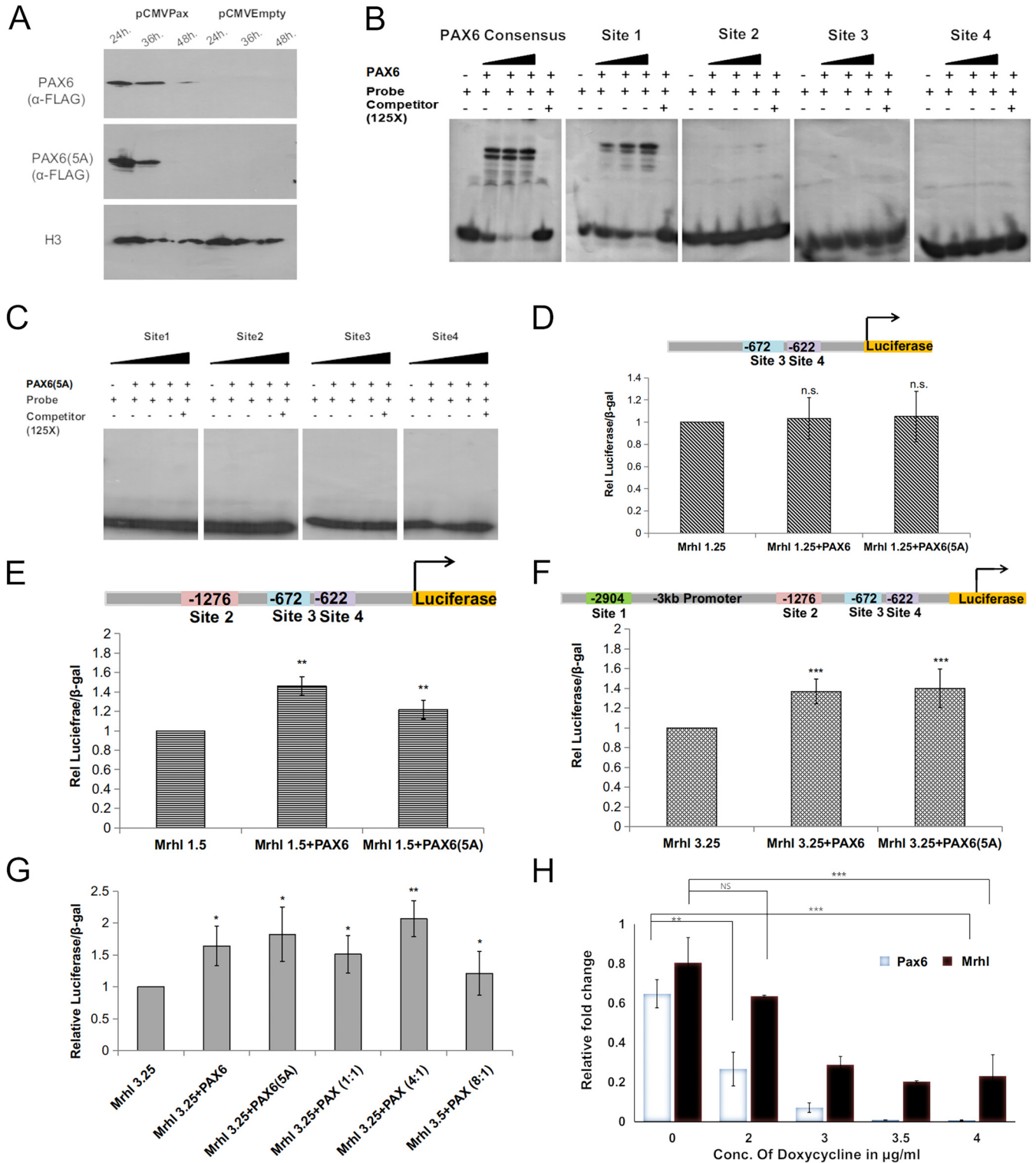


FIG 5 PAX6 physically binds to and regulates Mrhl in neuronal progenitors. (A) Expression and validation of PAX6 and PAX6(5A) by Western blotting. (B) EMSA for studying direct interaction of PAX6 on Mrhl promoter sites 1 to 4 revealed that PAX6 binds with high affinity to site 1 and with weak affinity to site 2. (C) EMSA for PAX6(5A) showed no binding to Mrhl promoter sites 1 to 4. (D to F) Luciferase assays for different constructs of the Mrhl promoter in the presence of exogenously expressed PAX6 and PAX6(5A) showed a site-dependent induction pattern. (G) Luciferase assay showing that PAX6/PAX6(5A) causes the highest induction of Mrhl at a ratio of 4:1. (H) Knockdown assay revealing a decrease in Mrhl expression upon knockdown of PAX6. Error bars indicate SD from three independent experiments, with technical duplicates in each ($n = 6$). *, $P < 0.05$; **, $P < 0.01$; ***, $P < 0.001$ (Student's t test).

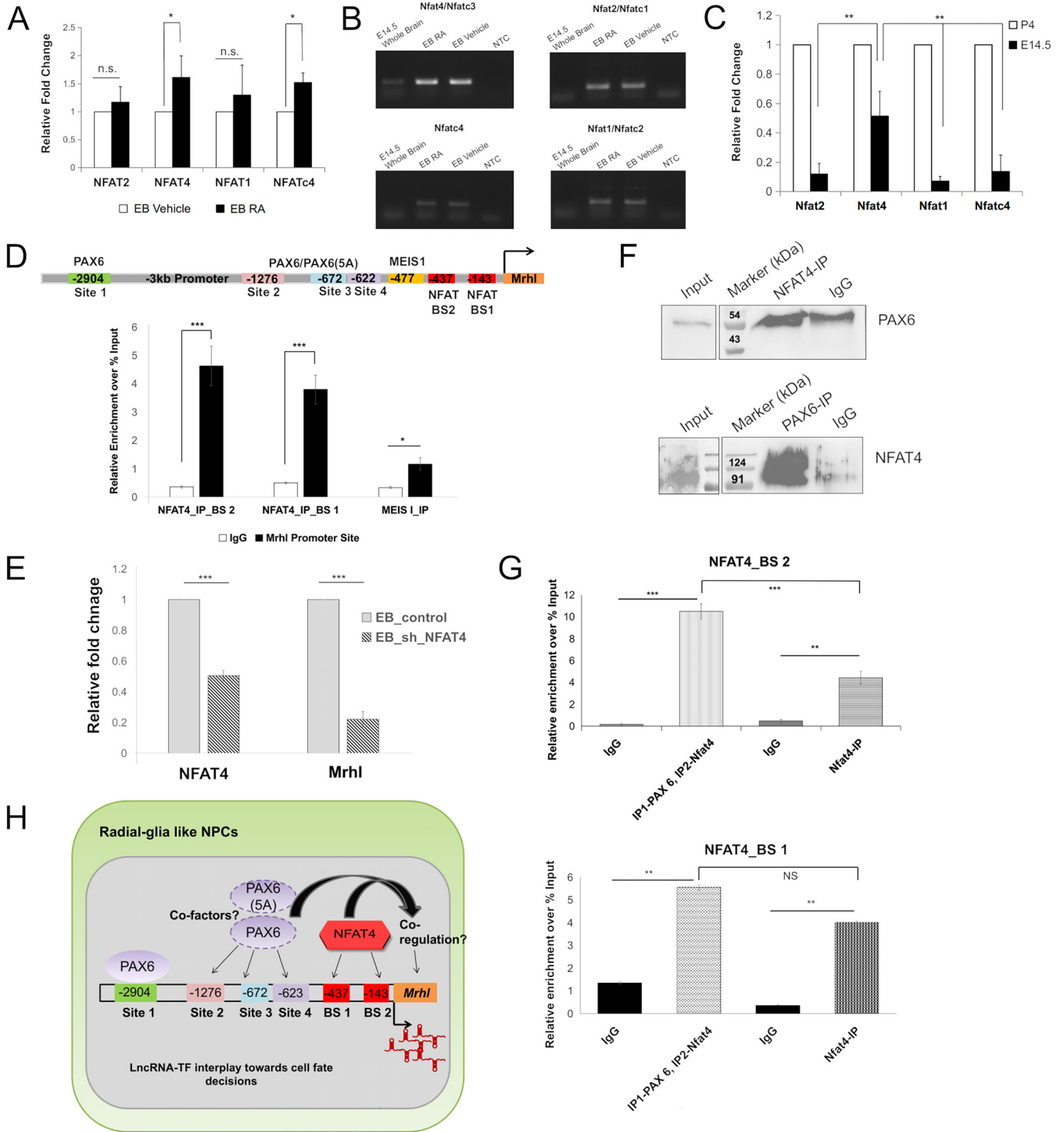


FIG 6 NFAT4 regulates Mrhl and binds to its promoter in association with PAX6. (A) Expression pattern of various NFAT isoforms in vehicle- versus RA-treated EBs. (B and C) Semiquantitative and quantitative PCR data, respectively, showing expression levels of isoforms of NFAT in E14.5 whole brain and EBs. Only NFAT4 is expressed highly in both the embryonic brain and EBs. NTC, no-template control. (D) ChIP-qPCR for NFAT4 and Meis1 binding on the Mrhl promoter showed ~4-fold-higher binding for NFAT4. (E) Knockdown of NFAT4 led to a reduction in expression of Mrhl. (F) ChIP-WB showed NFAT4 coprecipitation with PAX6 and vice versa. (G) Sequential ChIP results revealed significant enrichment for NFAT4 at BS 2 in PAX6-bound chromatin. (H) Model depicting the interplay between the Mrhl promoter and TFs, PAX6, and NFAT4 in NPCs, illustrating lncRNA-TF interactions in regulating cell fate decisions. Error bars indicate SD from three independent experiments, with technical duplicates in each ($n = 6$). *, $P < 0.05$; **, $P < 0.01$; ***, $P < 0.001$ (Student's t test).

cell types in the brain than their protein-coding counterparts. The roles of many lncRNAs, such as Dali, Paupar, Evf2, Rmst, and Pnky, to name a few, in regulating neural progenitor proliferation and/or differentiation and gene regulation have already been reported, with new additions every year (32, 71–77). A recent study demonstrated that the lncRNA SenZfp536 suppresses proliferation of cortical NPCs by *cis*-regulating the protein-coding gene *Zfp536* via chromosomal looping (78), while in another study (79), the lncRNA Neat1 was found to induce neuron-specific differentiation and to promote migration ability in spinal cord neural stem cells of mice by regulating WNT/ β -catenin signaling. In that study, the authors also gave evidence of regulation of lncRNA Neat1 expression by miR-124 (79). A study by Zhang et al. showed that the expression level of lncRNA Rik-203 increased during neural differentiation. Their data suggest that it facilitates neural differentiation by inhibiting miR-101a-3p's ability to reduce GSK-3 β levels (80).

The role of lncRNA Mrhl in development and differentiation was established in our previous studies (35, 36, 38). Nucleus-restricted Mrhl RNA has a definitive role in differentiation of B-type spermatogonial cells into meiotic spermatocytes, by negatively regulating the WNT signaling pathway, which is activated in differentiated meiotic spermatocytes, in association with p68/DDX5 helicase (35). On the other hand, in the context of mES cells, shRNA-mediated depletion and subsequent transcriptome analysis have revealed genes related to developmental processes, lineage-specific transcription factors, and key networks to be dysregulated, along with aberrance in specification of early lineages during differentiation of mES cells (38). Interestingly, the category of "development processes" in gene ontology analysis was observed to be overrepresented with the maximum number of dysregulated genes, most of them being related to the neuronal lineage. Furthermore, the nervous system also emerged as one of the perturbed clusters in gene coexpression analysis. Genome-wide chromatin occupancy studies further predicted that important neuronal TFs such as POU3F2 and FOXP2 are directly regulated at the chromatin level by Mrhl RNA. Our present study further confirmed that Mrhl is a key molecular player in neuronal lineage development.

Neuronal differentiation is a highly complex process which requires intertwined actions of various signaling pathways and transcription factors involved in regulating diverse aspects of neural stem cell/progenitor specification and maintenance as well as neurogenesis. The fact that the peak of lncRNA Mrhl expression at E14.5 is concurrent with the peak of neurogenesis in mouse brain development, along with the abrupt inhibition of Mrhl expression from postnatal stage P0 onward, is intriguing. This is also observed in the RA-induced neuronal differentiation model system. We also observed that depletion of Mrhl leads to premature commitment of NPCs to neurons, implying that balanced levels of Mrhl are required for the maintenance of NPCs. More importantly, it implies that downregulation of Mrhl is important for commitment of NPCs to differentiated neurons, in parallel with our studies in spermatogonial progenitors, where Mrhl levels need to be decreased for meiotic commitment to proceed. Our studies thus draw a common signature across model systems wherein Mrhl is required during initial differentiation for the development of progenitor cells but its downregulation is crucial for final commitment of progenitor cells to their differentiated types. Similar observations were also obtained in the study by Lv et al. (23), where transcriptomics analysis revealed restricted embryonic expression of many lncRNAs. For example, they detected an intronic lncRNA (chromosome 15, positions 66090924 to 66092050) which is highly expressed in early embryonic stages and whose expression is decreased to a basal level from E17.5. As another example, they also identified lncRNA Zfhx2as with increasing expression in E13 to E16, peaking at E17 while exhibiting only basal expression in the brain after birth. They concluded that embryonic restricted expression of lncRNAs have regulatory roles in the developing brain (23). It would be most interesting to delineate the mechanism of this shutting off of Mrhl expression in the post-natal brain as well as in the maturing neurons in the RA model system.

The mechanisms regulating this developmental stage-specific expression of lncRNAs are still not fully understood. However, studies have indicated that chromatin state, including

the cross talk between DNA methylation and histone modification, might be one of the mechanisms (23, 81, 82). It has also been reported that miRNAs, promoter-associated ncRNAs (pancRNAs), the specific location of lncRNAs with respect to protein-coding genes, and sometimes the transcript itself are involved in modulating their expression in a cell- and stage-specific manner (79–83). lncRNAs also seem to be regulated by the same set of transcription factors that influence the expression of protein coding genes. A transcriptomic profile study on mouse retinal photo receptor cells, done at six developmental time points in mice, revealed that regulation of ~20% of expressed lncRNAs is under the control of the rod differentiation factor, neural retina leucine zipper (NRL), predicting their role in development and differentiation of rod cells (84).

Regulation of lncRNAs by various TFs in cancers has also been reported recently (85, 86). As mentioned above, direct binding and transcriptional regulation of lncRNAs by key mES cell TFs, OCT4 and NANOG, have been reported to modulate the pluripotency of ES cells (26). In our efforts to identify key TFs that regulate the differential expression of Mrhl RNA during neuronal development, our bioinformatics analysis revealed the presence of PAX6 binding sites in the region upstream of the Mrhl gene which were also occupied by the PAX6 protein at the chromatin level. PAX6 is an important pioneer transcription factor that has a proven role in the regulation of neural development (59, 60). PAX6 is also a unique transcription factor in that it does not have a definite cognate DNA binding site but has a set of 10 overlapping DNA binding motifs which function in a very context-dependent manner (62). Our extensive analysis presented here shows that among the four PAX6-occupied DNA binding sites, site 1, situated 2.9 kb upstream of Mrhl TSS, is relevant for the direct regulation of Mrhl expression in NPCs. Since this PAX6 binding site is far upstream of the TSS, we argued that PAX6 might interact with one transcription factor that binds to the proximal promoter region. This assumption was also based on reports showing that PAX6 may not act in isolation but may interact with other TFs to regulate target genes. PAX6 forms a ternary complex with SOX2 and occupies lens-specific enhancer elements, leading to the initiation of lens development (65). In neural progenitor cells, PAX6 acts in cooperation with SOX2 to bind and regulate common target genes (60). PAX6 has also been shown to coimmunoprecipitate with methyl transferases such as MLL1 and MLL2, acting to recruit these chromatin remodelers to target enhancers (87).

In our study, we found that PAX6 associates with NFAT4 in the same chromatin complex, as shown by ChIP-WB and sequential ChIP assays, and they may act in conjunction to regulate Mrhl expression in NPCs. It is interesting that NFAT4 is also a neuronal-lineage-specific transcription factor (69, 70). Another major observation made in the present study is that WNT signaling is not involved in the regulation of the Mrhl gene in RA-derived NPCs, which is in contrast to its role in B-type spermatogonial cells. Thus, it is likely that the Mrhl gene is regulated by different sets of transcription factors in a lineage-specific manner.

The regulation of lncRNA Mrhl by PAX6/PAX6(5A) through multiple sites of action in NPCs, independently or in probable conjunction with cofactors, suggests an intriguing interplay of lncRNAs and proteins in coordinating cell-specific events. However, recognizing the complexity in lineage specification and interplay between several regulation factors, we also cannot rule out the possibility that other TFs or cofactors may also be involved in this mechanism. For example, we found the presence of RARE (retinoic acid response element) sites on the 3-kb-upstream promoter region for Mrhl. In the context of the RA-induced neuronal model system, this is worthy of exploration. Furthermore, it would be interesting to investigate whether Mrhl-PAX6-NFAT4 interaction dynamics is important for the maintenance of the NPC pool during embryonic brain development as well as to probe into other factors that are involved in the aforementioned dynamics. It would be particularly interesting to delineate the chromatin-based mechanisms behind regulation of Mrhl by these two TFs in NPCs.

The regulation of spatial and temporal expression of lncRNAs indeed adds to their functional role in context-specific manner. Expression of the lncRNA Mrhl itself is

restricted to the testes, livers, kidneys, and spleens of adult mice (33, 34). Its expression in mouse ES cells and spermatogonial progenitor cells signifies its role in development (35, 36, 38). The present study shows that the expression of Mrhl is restricted to embryonic stages of brain and NPCs, with minimal basal levels in maturing neurons and post-natal brain. At this juncture, an important question that needs to be addressed is the biological relevance of differential expression of Mrhl RNA during neuronal development. The approach of transcriptome analysis in NPCs depleted of Mrhl should give valuable information about the gene targets of Mrhl RNA in NPCs. We add here that the gene targets of Mrhl lncRNA are quite different in mouse spermatogonial cells and mES cells (36, 38), indicating that the gene targets are cell type specific and context dependent. Thus, the present study has demonstrated an unexpected new role for lncRNA Mrhl in neuronal development. Future studies on the molecular and cellular functions of Mrhl lncRNA in neuronal development should add to the diversity of cellular functions exhibited by this lncRNA.

MATERIALS AND METHODS

Cell lines, plasmids, reagents, and oligonucleotides. The E14TG2a feeder-independent mouse ES cell line was a kind gift from Tapas K. Kundu's lab (JNCASR, India). Mouse ES cells were maintained on 0.2% gelatin (Himedia, TC041)-coated dishes and grown in high-glucose Dulbecco's modified Eagle medium (DMEM) (Sigma, D1152), 15% fetal bovine serum (FBS) (Gibco, 16000-044), 1× nonessential amino acids (Sigma, M7145), 0.1 mM β -mercaptoethanol, and 1× penicillin-streptomycin (Sigma, P4333) supplemented with ESGRO (Merck Millipore). The P19EC line was a kind gift from Kumar Somasundaram's lab (IISc, India), and cells were grown in DMEM, 10% FBS, 0.1 mM β -mercaptoethanol, and 1× penicillin-streptomycin. The HEK293T cell line (ATCC, USA) was maintained in DMEM, 10% FBS, and 1× penicillin-streptomycin. All cell lines have been tested and determined to be free of mycoplasma contamination using a PCR kit (Applied Biological Materials Inc., G238).

Mrhl shRNA sequences are as follows: Mrhl shRNA#1, 5'-GCACATACATACATACATATATT-3'; Mrhl shRNA#4, 5'-GGAGAAACCTCAAAGTATT. PAX6 shRNA (in the SMART vector inducible lentiviral backbone) clone was obtained from Horizon Discovery (clone ID V3IMPPGG_11530401). Nfat4/Nfatc3 shRNA (in the SMART vector inducible lentiviral backbone) clone was obtained from Horizon Discovery (clone ID V3SM7671-232277435). p3x-FLAG-CMV-10 (Sigma) was used for the generation of PAX6 and PAX6 (5A) expression vectors. PAX6 and PAX6(5A) were amplified from cDNA of E14.5 mouse embryonic brains and cloned into the vector. pGL4.10 (luc2) vector (Promega, E6651) was used for the generation of Mrhl promoter constructs for luciferase assays. 1.25 kb, 1.5 kb or 3.25 kb of the Mrhl promoter (250 bp were taken downstream of the transcription start site in each case) were amplified from genomic DNA and cloned into the vector. All fine chemicals were obtained from Sigma (unless otherwise mentioned), gelatin was obtained from Himedia, and FBS was obtained from Gibco (Performance Plus; U.S. origin). Oligonucleotide sequences and antibodies are listed in Tables 2 and 3, respectively.

Animal procedures. CD-1 strain mice (*Mus musculus*) were used for isolating embryonic and post-natal brains at indicated stages. For embryonic brain isolation, female mice at age 6 to 8 weeks were bred with males and were checked for plugs to confirm mating. The day of detection of the plug was considered 0.5 day postcoitum (dpc). All animal procedures were performed in accordance with the Institutional Animal Ethics Committee of JNCASR, India.

Transfection/transduction protocols. Transfections for P19EC and HEK293T cells were performed using Lipofectamine 2000 (Thermo Fisher Scientific, 11668019) as per the manufacturer's protocol. Transduction of mES cells was performed as per the protocol of Pijnappel et al. (88). Briefly, HEK293T cells were transfected with 5 μ g PAX6 shRNA plasmid, 2.5 μ g pSPAX2, 1.75 μ g pVSVG, and 0.75 μ g pRev to generate the viral particles. The medium containing viral particles was harvested 48 h after transfection. A second round of viral particles was collected after an additional 24 h. The viral supernatant was mixed with 8 μ g mL⁻¹ DEAE-dextran and 1,000 U mL⁻¹ ESGRO and added directly to the E14TG2a cells. Transduction was performed for 24 h with the first round of viral particles and an additional 24 h with the second round of viral particles. The transduced cells were then subjected to puromycin selection (1.5 μ g mL⁻¹ puromycin) for a week.

Neuronal differentiation of mES cells. The protocol described by Bibel et al. (45) was followed for RA-mediated neuronal differentiation of mES cells. Cells (4×10^6) were plated onto 100-mm bacteriological-grade dishes (Greiner Bio-One, 633102) in differentiation medium containing DMEM, 10% FBS, 0.1 mM β -mercaptoethanol, and 1× penicillin-streptomycin and allowed to grow for 4 days. RA (Sigma, R2625) or dimethyl sulfoxide (DMSO) (Sigma, D2650) was added to the EBs on the fourth day at a final concentration of 5 μ M, and cells were allowed to grow for an additional 4 days. After a total of 8 days of differentiation (4-/4+ RA), the RA- and DMSO-treated EBs were harvested by gravity precipitation for cryosectioning. Alternatively, RA-treated EBs were trypsinized to obtain NPCs with 0.05% freshly made trypsin for 3 min at 37°C, dissociated, and filtered through 40- μ m filters (Falcon, 352340). NPCs were collected by centrifugation at 1,150 rpm for 5 min.

For the generation of early and maturing neurons, plates or coverslips were coated with 100 μ g mL⁻¹ poly-D-lysine (Merck Millipore, A-003-E) at 37°C overnight. Next day, plates were washed thoroughly three times with deionized sterile water and dried. The plates were then coated with laminin solution (Roche, 11243217001) for 2 h at 37°C and kept ready for use. The cell pellet obtained as described

TABLE 2 Primer and oligonucleotide sequences

Use	Primer(s) (5' to 3')	
	Forward	Reverse
qRT-PCR		
Nestin	GTCGTTAGAGGTGCAGCAG	TTCAGGATCTGAGCGATCT
PAX6	TCCAGGTGCTGGACAATGAA; CGGCTTCCCACAACCTCTATC	GCTTTTCGCTAGCCAGGTG; ACCGCCCTTGGTTAAAGTCT
Ascl1	TGCGGCTGCTTTCCTTTTC	CTCGAAGCACGATCAAAGG
Tuj1	TGAGGCTCTCTCAACAAGT	CCAGCACCACTCTGACCCAAA
GFAP	CACGAA CGAGTCCCTAGAGC	GTGGCCTTCTGACACGGATT
Hes5	GAGATGCTCAGTCCCAAGGAG	GCGAAGGCTTGTGTGTTT
Mrhl	TGAGACCATGGCTGGACTCT; CTGCACACACAAAACACACA	AGATGCAGTTTCCAATGTCCAAAT; AGGGTTCTCTGTCTCTGACCT
FoxG1	GGCAAGGGCAACTACTGGAT	CGTGGTCCCGTTGTAECTCA
En1	TCTACTCATGGTTTCGGCT	CTGGAACCTCCGCCCTTGAGTC
Gbx2	CAACTTCGACAAAAGCCGAGG	TGACTCGTCTTCCCTTGCC
Nfatc1/NFAT2	ACCGATAGCACTCTGGACT	GTCCGGGAAAGAGACTTGGG
Nfatc3/NFAT4	TCAGTCAATGCACAGCCTTT	AGGTGGGGTTTTGCACAGAAT
Nfatc2/NFAT1	CCAAGACGAGCTGGACTTTTC	GCATCAGTTCGTGGATGGA
Nfatc4	TGGTTATAGCACACCCGCTC	CTCAGGAGGTAAGGGGTGGA
β -actin	AGGTCATCACTATTGGCAACG	TACTCCTGCTTGTGATCCAC
Map2	TGCCCTTGGGTTTAACTTTG	CCTTCATCCATGCTTCCACT
NeuN/Rbfox3	TCGTAGGCTCCGTTCTGCT	AGACCCACAGCACCTTGACT
NFAT4	CACAGCCCAAGTGGAAGAAGTT	GGGAGTTCTTGAGCAGATCG
ChIP		
Mrhl PAX6 ChIP site 1	TCCACCTTACTTGCCTTGGGA	CAGTCATTTGGGAAGGTTGCT
Mrhl PAX6 ChIP site 2	GGTCTTCTTCTCTGAGTTTAATGTG	GGGTTGCTATCTTGCCACT
Mrhl PAX6 ChIP sites 3 + 4	TTCATGTGCTGTGTATACCTCTTCA	TTTCCTTCTTAAACTGTTTCTCTG
Mrhl proximal promoter (histone ChIP)	GAACTCCAGCCTATCTGATGGT	GCGATTATCTGGTAAAGCACACC
Actin ChIP	CACCCATCGCCAAAACCTTTCAT	CGCACAGTGCAGCATTTTTTTTAC
Mrhl Meis1 and NFAT4 BS2 ChIP	TTCATCCAAGGAGGGAGTGT	GGCTGGAGTTCAGGACAAAG
Mrhl TCF4 and NFAT4 BS1 ChIP	AGAAATCCGCCTGCCTCT	GATGCCAGCATTTTTACAGCA
EMSA		
Site 1	CTGTAATCTTAAAITATGCATCCTTCCGTGCACCTGACAC	GTGTCAGGTGCAGGAGGATGCATAAITTAAGATTACAG
Site 2	AGAAAAATCATCAGCTAGGAGAAAATGATAAAATTTACT	AGTAAATTTATCATTTTCTCTAGACTGATGATTTTTTCT
Site 3	CATTATCTTCTAAAATCTTCATGTGTCTGTATACCTC	GAGGTATACACAGACACATGAAGAAATTTAGAAAAGATAATG
Site 4	TCCTCTTAGCAAGAGCAGTGGTTACTTTTTGTGTTTTAT	ATAAAAACAAAAAGTAACCACTGCTCTTCTAGGAGA
PAX6 positive control	GGATGCAATTTACCGCATGAGTGCCTCGAGGGATCCAGGTCCA	TCCAGGTGGATCCCTCAGGCACTCATGGTGAATTTGCATCC

TABLE 3 Antibodies

Antibody target	Company	Catalogue no.	Dilution used
PAX6	Abcam	ab5790	1:500 for IF; 5 μ g for ChIP per 25 μ g of chromatin
Nestin	Abcam	ab11306	10 μ g/mL for IF
Tuj1	Abcam	ab14545	1:1,000 for IF
β -Catenin	Abcam	ab32572	1:250 for IF
NICD	Abcam	ab8925	1:250 for IF
H3K4me3	Abcam	ab12209	5 μ g for ChIP per 25 μ g of chromatin
Meis1	Millipore	ABE2864	5 μ g for ChIP per 25 μ g of chromatin
NF-ATC3	Abcam	ab83832	1:500 for WB; 5 μ g for ChIP per 25 μ g of chromatin

above was resuspended in N2 medium containing DMEM-F-12 (Sigma, D2906), 1 \times N2 (Thermo Fisher Scientific, 17502048), and 1 \times penicillin-streptomycin and plated at a density of 90,000 cells cm⁻². N2 medium was changed 2 h after plating and then again after 24 h. For further differentiation, medium was changed after an additional 24 h to N2B27 medium containing DMEM-F-12, 1 \times N2, 1 \times B27 (Thermo Fisher Scientific, 17504044), and 1 \times penicillin-streptomycin. Cells were harvested at different time points for appropriate analyses.

PAX6 knockdown and Mrhl expression. A PAX6 shRNA clone was used to generate a stable inducible mES cell line. The protocol for RA-mediated neuronal differentiation of mES cells described above was followed. PAX6 knockdown was induced by addition of different concentrations of doxycycline (0, 2, 3, 3.5, and 4 μ g mL⁻¹) from day 3 onward, every day. RA was added on the fourth day, and EBs were harvested on day 5. RNA was isolated from collected cells, and qPCR was performed as described below for expression of PAX6 and Mrhl.

NFAT4 knockdown and Mrhl expression. An NFAT4 shRNA clone was used to generate stable inducible mES cell line. mES cells were directly transduced with lentiviral particles obtained from Horizon Discovery at a multiplicity of infection (MOI) of 4. Puromycin was used to select the transfected cells. The protocol for RA-mediated neuronal differentiation of mES cells described above was followed. NFAT4 knockdown was induced by addition of 3.5 μ g mL⁻¹ doxycycline from day 3 onward, every day. RA was added on day 4, and EBs were harvested on day 5. RNA was isolated from collected cells, and qPCR was performed as described below for expression of NFAT4 and Mrhl.

NOTCH inhibition studies. EBs were treated with the NOTCH inhibitor DAPT [*N*-[*N*-(3,5-difluorophenyl)-*L*-alanyl]-*S*-phenylglycine *t*-butyl ester; Sigma, D5942] at a concentration of 10 μ M on the fourth day of differentiation along with RA. EBs were harvested on the fifth day and processed directly for qPCR as described below.

Preparation of NPC smears. EBs were trypsinized and filtered as described earlier and cross-linked with 1% formaldehyde for 8 min at room temperature. Formaldehyde was quenched using 1/7 volume of 1 M glycine for 5 min at room temperature, and cells were collected by centrifugation at 1,500 rpm for 5 min at 4°C. The cells were washed 3 times with ice-cold 1 \times phosphate-buffered saline (PBS) and collected by centrifugation each time. A 10- μ L aliquot of the cell suspension in 1 \times PBS was placed on a slide, covered with a coverslip, and dipped in liquid N₂ to fix the cells on the slide (aliquot volume can be determined empirically to obtain desired cell density per aliquot). The coverslip was removed immediately thereafter with the help of a scalpel blade. The slides were hydrated in 1 \times PBS for 3 to 5 min and dehydrated in graded ethanol from 50%, 75%, and 95% to 100%. The slides were stored in 100% ethanol at this point. Before proceeding with RNA FISH or IF, slides were rehydrated in the reverse order of ethanol series with a final rehydration step in 1 \times PBS.

RNA FISH and IF. RNA FISH followed by IF on EBs, NPCs, or brain tissues was performed as per the protocol of de Planell-Saguer et al. (89). The probes used for RNA FISH were Cy5-labeled locked nucleic acid probes procured from Exiqon (35) with the sequence 5'-CAGCTAGGCCAAGACAACAAAATG-3'.

(i) Fixation and permeabilization. Cells were grown on coverslips, or cell smears were prepared as described above. EBs or brain tissues were fixed in 4% paraformaldehyde for 7 to 8 h at 4°C followed by equilibration in 20% sucrose solution overnight and embedded in tissue-freezing medium (Leica, 14020108926). The embedded tissues were then cryosectioned and collected on Superfrost slides (Fisher Scientific, 12-550-15). For cells, a brief wash was carried out with 1 \times PBS (pH 7.4) followed by fixation with 2% formaldehyde for 10 min at room temperature. The cells were then washed with 1 \times PBS three times for 1 min each, permeabilization buffer (1 \times PBS, 0.5% Triton X-100) was added for 5 min, and cells were incubated at 4°C. The permeabilization buffer was removed, and cells were washed briefly with 1 \times PBS for three times at room temperature. For tissue sections, antigen retrieval was performed by boiling the sections in 0.01 M citrate buffer (pH 6) for 10 min. The sections were allowed to cool and were washed in distilled water three times for 5 min each and then in 1 \times PBS for 5 min, each time with gentle shaking.

(ii) Hybridization. The samples were then blocked in prehybridization buffer (3% bovine serum albumin [BSA], 4 \times SSC [1 \times SSC is 0.15 M NaCl plus 0.015 M sodium citrate, pH 7]) for 40 min at 50°C. Hybridization (Mrhl probes tagged with Cy5; final concentration, 95 nM) was performed with prewarmed hybridization buffer (10% dextran sulfate in 4 \times SSC) for 1 h at 50°C. After hybridization, slides were washed four times for 6 min each with wash buffer I (4 \times SSC, 0.1% Tween 20) at 50°C followed by two washes with wash buffer II (2 \times SSC) for 6 min each at 50°C. The samples were then washed with wash

buffer III ($1 \times$ SSC) once for 5 min at 50°C followed by one wash with $1 \times$ PBS at room temperature. For tissue sections, all washes were performed as mentioned above with a time of 4 min for buffers I to III. The samples were then processed for IF.

(iii) IF. Samples were blocked with IF blocking buffer (4% BSA, $1 \times$ PBS) for 1 h at 4°C. Primary antibody solution (2% BSA, $1 \times$ PBS) contained the appropriate dilution of the desired primary antibody, and the samples were incubated in it for 12 h at 4°C. Next day, the samples were washed with IF wash buffer (0.2% BSA, $1 \times$ PBS) three times for 5 min each with gentle shaking. The samples were incubated in secondary antibody for 45 min at room temperature and washed with $1 \times$ PBS three times for 10 min each with gentle shaking. The samples were finally mounted in mounting medium containing glycerol and DAPI (4',6-diamidino-2-phenylindole) and imaged on a Zeiss LSM 510 Meta microscope.

ChIP. ChIP was performed according to Cotney and Noonan's protocol (90). Protein A and protein G Dynabeads (Thermo Fisher Scientific, 10001D and 10003D) were used for rabbit and mouse antibodies, respectively. For ChIP-WB, the same protocol was followed, and whole samples after IP were processed for Western blotting.

(i) Preparation of antibody beads. Twenty-five microliters of Dynabeads was used for each ChIP reaction. The beads were first washed with 1 mL of bead binding buffer ($1 \times$ PBS, 0.2% Tween-20) and resuspended in 200 μ L of the buffer per reaction. H3K4me3 (2 μ g) or PAX6 (4 μ g) antibodies or their isotype controls were added to the beads in separate tubes and incubated for \sim 16 h at 4°C on an end-to-end rotor at 10 rpm. The next day, beads were washed with 1 mL of bead binding buffer followed by 1 mL of dilution buffer (0.01% SDS, 1.1% Triton X-100, 1.2 mM EDTA, 16.7 mM Tris-HCl [pH 8.1], 167 mM NaCl). The beads were then resuspended in 25 μ L dilution buffer per ChIP reaction and stored at 4°C for further use.

(ii) Chromatin extraction and quantification. Brain tissues from E14.5 embryos or EBs were harvested in serum-free DMEM. Brain samples were minced with a scalpel blade, and a homogeneous suspension was obtained with the help of a pipette. EBs were trypsinized and filtered as described above. The samples were then subjected to cross-linking using 1% formaldehyde (Sigma, F8775) for 10 min at room temperature, following which samples were quenched with glycine at a final concentration of 0.125 M for 10 min at room temperature. The samples were then centrifuged at $2,000 \times g$ for 10 min at 4°C and washed twice with $1 \times$ ice-cold PBS. Finally, the pellets were either flash frozen in liquid N₂ and stored at -80°C or processed for chromatin extraction.

The cross-linked pellet was resuspended in 6 volumes of ice-cold cell lysis buffer (50 mM Tris-HCl [pH 8.0], 140 mM NaCl, 1 mM EDTA, 10% glycerol, 0.5% NP-40, 0.25% Triton X-100) supplemented with $1 \times$ mammalian protease inhibitor cocktail and incubated on ice for 20 min. For brain samples, the pellets were homogenized once after addition of lysis buffer with 30 to 40 strokes (BioSpec Tissue-Tearor; 985370) and once after the incubation period was over. The nuclei were then harvested by centrifugation at $2,000 \times g$ for 5 min at 4°C. The supernatant was removed, and the nuclei were resuspended in 5 volumes of ice-cold nuclear lysis buffer (10 mM Tris-HCl [pH 8.0], 1 mM EDTA, 0.5 mM EGTA, 0.5% SDS) supplemented with $1 \times$ mammalian protease inhibitor cocktail and incubated on ice for 20 min. The samples were then sonicated in a Bioruptor device (Diagenode, UCD-200) for 35 cycles (at pulses of 30 s on and 30 s off) and centrifuged at $16,000 \times g$ for 10 min at 4°C to remove insoluble material. The centrifuged samples were then transferred to fresh tubes, aliquoted as per requirement, flash frozen in liquid N₂ and stored at -80°C .

For monitoring sonication efficiency and DNA quantification, 10- μ L aliquots were kept aside, diluted in 10 μ L of Tris-EDTA (TE) buffer, and treated with 10 μ g of RNase A (Sigma, R6513) for 30 min at 37°C followed by 20 μ g of proteinase K (Thermo Fisher Scientific, E00491) for 1 h at 55°C. The aliquots were then subjected to reverse cross-linking for 5 min at 95°C, allowed to cool to room temperature slowly, and analyzed on 1% agarose gels for sonication efficiency or subjected to DNA isolation by the phenol-chloroform method for quantification.

(iii) Immunoprecipitation. Approximately 10 to 25 μ g of chromatin was diluted with dilution buffer supplemented with $1 \times$ mammalian protease inhibitor cocktail to reduce the SDS concentration to $<0.1\%$ and achieve a final volume of 450 μ L. Then, 5% of the dilution was stored as input at 4°C. Twenty-five microliters of antibody or isotype control beads was added to the chromatin dilution and incubated for 12 to 16 h at 4°C. Next day, the beads were washed with 1 mL wash buffer (100 mM Tris-HCl [pH 8.0], 500 mM LiCl, 1% NP-40, 1% deoxycholic acid) supplemented with $1 \times$ mammalian protease inhibitor cocktail 5 times at room temperature. The beads were given a final wash with 1 mL of TE buffer and resuspended in 85 μ L of elution buffer (50 mM Tris-HCl [pH 8.0], 10 mM EDTA, 1% SDS). Elution was performed twice for 10 min each at 65°C under constant agitation in a thermal mixer. All ChIP and input samples (volume made up to 170 μ L with dilution buffer for input samples) were subjected to reverse cross-linking for 12 h at 65°C.

(iv) Chromatin purification and analysis. Next day, all samples were treated with 10 μ g of RNase A for 1 h at 37°C followed by 200 μ g proteinase K for 2 h at 55°C, and DNA was extracted by the phenol-chloroform method. The DNA was precipitated with 1/10 volume 3 M sodium acetate (pH 5.2), 3 volumes of 100% ethanol, and glycogen at a final concentration of 0.5 μ g μL^{-1} overnight at -20°C . Next day, DNA was pelleted, washed with 75% ethanol, dried, dissolved in sterile deionized water, and subjected to qRT-PCR analysis.

ChIP-WB. ChIP was performed according to Cotney and Noonan's protocol (90). Briefly, cross-linked EBs were sonicated, and 50 μ L of sonicated samples was kept aside at -80°C as input. Each sample (150 μ L, for each IP and respective IgG) was then diluted approximately $6 \times$ to get a volume of 1 mL in ChIP dilution buffer (0.01% SDS, 1.1% Triton X-100, 1.2 mM EDTA [pH 8.0], 16.7 mM Tris-Cl [pH 8.0], 167 mM NaCl). Samples were incubated overnight at 4°C on rotor with 5 μ g of respective antibody. Next

day, 30 μL of protein G Dynabeads (Thermo Fisher Scientific, 10004D) was hybridized with the samples for 2.5 h after equilibrating with ChIP dilution buffer. After hybridization, beads were washed with low-salt buffer (0.1% SDS, 1% Triton X-100, 2 mM EDTA [pH 8.0], 20 mM Tris-Cl [pH 8.0], 150 mM NaCl) once, high-salt buffer (0.1% SDS, 1% Triton X-100, 2 mM EDTA [pH 8.0], 20 mM Tris-Cl [pH 8.0], 500 mM NaCl) once, LiCl buffer (0.25 M LiCl, 1% IGEPAL, 1% deoxycholic acid, 1 mM EDTA [pH 8.0], 10 mM Tris-Cl [pH 8.0]) once, and TE buffer twice. After washing, beads were resuspended in 40 μL of 6 \times loading dye, and the samples along with the input were boiled for 10 min and then stored at -20°C for later use. A 10% SDS gel was used to resolve the protein bands, and Western blotting was performed to get the final results.

Sequential chip or ChIP-re-ChIP assays. The protocol described by Furlan-Magaril et al. (91) was followed, with a few modifications. For the first round of IP, sonicated and ChIP buffer-diluted samples were incubated with two antibodies specific to our two proteins of interest (PAX6 and NFAT4) along with their IgG controls, and the rest of the ChIP protocol was then followed. For re-ChIP, the elution of complexes during the first ChIP was carried out using 50 μL of 10 mM dithiothreitol (DTT) at 37°C for 40 min. After elution, the beads were separated, and the eluate was diluted 20 times with re-ChIP buffer (1% Triton X-100, 2 mM EDTA, 150 mM NaCl, 20 mM Tris-HCl [pH 8.1]) and subjected again to the ChIP procedure with alternate antibodies along with ChIP for NFAT4-IP alone. Finally, DNA was extracted from eluted samples using the phenol-chloroform method, and qRT-PCR was done for further analysis.

Purification of PAX6 and PAX6(5A) proteins. p3X-FLAG-CMV-10-Pax6 and -Pax6(5a) constructs were transfected into HEK293T cells. Twenty-four hours after transfection, cells were lysed in 5 volumes of FLAG lysis buffer (50 mM Tris-HCl [pH 7.4], 150 mM NaCl, 1 mM EDTA, 1% Triton X-100) supplemented with 1 \times mammalian protease inhibitor cocktail. To 500 μL of supernatant containing proteins, 30 μL M2 agarose beads (Sigma, A220) was added, and the mixture was incubated for 3 h at 4°C . The beads were then washed in 1 mL of FLAG wash buffer (50 mM Tris-HCl [pH 7.4], 150 mM NaCl). The FLAG-tagged proteins were then eluted in the FLAG wash buffer containing a final concentration of 500 ng μL^{-1} of FLAG peptide (Sigma, F4799).

EMSA. (i) End labeling of probe and purification. Oligonucleotides were designed such that they harbored the PAX6/PAX6(5A) motifs on the Mrhl promoter. All forward oligonucleotides were subjected to end labeling with [γ - ^{32}P]ATP in polynucleotide kinase (PNK) reaction buffer (PNK buffer at a final concentration of 1 \times is 40 pmol oligonucleotide, 20 U PNK [New England Biolabs, M0201S], and 30 μCi [γ - ^{32}P]ATP, with the volume made up to 50 μL with nuclease free water) for 30 min at 37°C . The enzyme was heat inactivated for 20 min at 65°C . The oligonucleotides were purified by the phenol-chloroform method and precipitated in 1/10 volume of 3 M sodium acetate (pH 5.2), 3 volumes of 100% ethanol, and 10 μg yeast tRNA for 1 h at -80°C . The oligonucleotides were pelleted by centrifugation at 12,800 rpm for 10 min, washed in 75% ethanol and dried. They were then dissolved in 1 \times annealing buffer (10 mM Tris-HCl [pH 8.0], 20 mM NaCl). To each of the forward oligonucleotides, a 3 \times excess of the reverse oligonucleotides was added, and the mixture was heated for 10 min at 95°C and allowed to cool slowly over several hours to overnight at room temperature. The annealed probes were purified using Sephadex C-50 columns. Glass wool was packed near the tip of a 1-mL syringe to a volume of 0.1 mL, and the syringe was packed with a C-50 bead slurry to a volume of 1 mL with centrifugation at 1,800 rpm for 3 min at 4°C . A final centrifugation was performed for the packed beads to remove all water before loading the annealed probes onto the column. The annealed probes were collected again by centrifugation, and their activity was recorded as counts per minute in a scintillation counter. Unlabeled forward oligonucleotides were also annealed to their corresponding reverse oligonucleotides and purified in a similar manner for competition assays.

(ii) Binding reaction and electrophoresis. The purified proteins were allowed to bind to the oligonucleotides in a reaction mix containing 5 \times EMSA buffer (60 mM HEPES-KOH [pH 7.9], 300 mM KCl, 15 mM MgCl_2 , 2.5 mM DTT, 20% [wt/vol] Ficoll 400, and 1 mg mL^{-1} BSA, with 1 \times mammalian protease inhibitor cocktail added just before use) to a final concentration of 1 \times , purified PAX6 or PAX6(5A) protein (100 to 400 ng in increasing concentrations), 400 ng μL^{-1} salmon sperm DNA (Sigma, D9156) and [γ - ^{32}P]ATP-labeled double-stranded oligonucleotide (20,000 cpm). The volume was made up to 12.5 μL with nuclease-free water. The reaction mixture was incubated for 40 min at 37°C . For competition assay, a 125 \times molar excess of unlabeled double-stranded probe was used. After incubation, loading dye (containing bromophenol blue and xylene cyanol without SDS) was added to the samples, and the samples were run on a 5% native gel (40% acrylamide stock in a 30:08 ratio of acrylamide to bis-acrylamide) prepared in 0.5 \times TBE (10 \times TBE stock is 1.8 M Tris base, 90 mM boric acid, and 2.5 mM EDTA) at 150 V at 4°C . The gel was then dried and exposed to X-ray film for 24 h.

Luciferase and β -galactosidase assay. P19EC cells were transfected with 2 μg of pGL4-Mrhl promoter constructs, 200 ng of PAX6 or PAX6(5A) expression plasmids, and 50 ng of β -galactosidase plasmid as an internal control. Cells were harvested 24 h posttransfection, and a luciferase assay was performed as per the manufacturer's protocol (Promega, E2610). Readings for luminescence were taken with a luminometer (Berthold, Sirius L).

The β -galactosidase assay as performed as described by Uchil et al. (92). Briefly, 30 μL of the cell extract was mixed with 3 μL 100 \times Mg^{2+} solution (0.1 M MgCl_2 , 4.5 M beta-mercaptoethanol), 66 μL 1 \times ONPG (4 mg mL^{-1} *o*-nitrophenyl- β -D-galactopyranoside in 0.1 M phosphate buffer [pH 7.5]) and 201 μL 0.1 M sodium phosphate (pH 7.5). The reaction mixtures were incubated for 30 min to a few hours at 37°C until a faint yellow color developed. The reactions were stopped by adding 500 μL 1 M Na_2CO_3 , and the absorbance was recorded at 420 nm in a spectrophotometer.

RNA isolation, qPCR, and Western blotting. Total RNA was isolated from cells or tissues using RNAiso Plus (TaKaRa Bio) for analysis by qRT-PCR as per the manufacturer's protocol. Real-time PCR was performed using Sybr green mix (TaKaRa) in a real-time PCR machine (Bio-Rad CFX96).

Cells or tissues were lysed in 5 volumes of radioimmunoprecipitation assay (RIPA) buffer (150 mM sodium chloride, 1.0% NP-40 or Triton X-100, 0.5% sodium deoxycholate, 0.1% SDS, 50 mM Tris-HCl [pH 8.0], 1 mM EDTA, 0.5 mM EGTA) supplemented with 1 mM phenylmethylsulfonyl fluoride (PMSF) and 1× mammalian protease inhibitor cocktail for 15 min on ice with occasional vortexing. Protein concentration was estimated using the Bradford reagent. Samples were resolved on 10 to 12% SDS-PAGE gels, transferred to nitrocellulose membrane, incubated with primary and secondary antibodies, and analyzed using chemiluminescence (Millipore, Luminata Forte, WBLUF0100) and exposure to X-ray films.

ChIP and FIMO analysis. Publicly available ChIP-Seq data sets, including GSE93009 (44) for RNA Pol II, RNA Pol II-Ser5p, H3K4me3, and H3K27me3 and GSE66961 (61) for PAX6, were used.

A 3-kb promoter sequence of Mrhl (upstream from its TSS) was taken, along with the motifs for PAX6 binding, as described in a report by Xie and Cvekl (62). FIMO (Find Individual Motif Occurrences) (93) scanning was then performed with a default cutoff value of $1E-04$.

Promoter analysis. GPMiner (50) and JASPAR (51) programs were used to analyze 3 kb upstream of the TSS of Mrhl. SnapGene software was used to map the binding sites of various TFs on the promoter region.

ACKNOWLEDGMENTS

We thank Suma B. Srinivas of the Confocal Imaging Facility, Prakash R. Gnaneshwar of the Animal Facility, and Anitha S. Rokhade of the Sequencing Facility at JNCASR, India.

M.R.S.R. acknowledges the Department of Science and Technology, Government of India, for a SERB Distinguished Fellowship and SERB-YOS (Year of Science Chair Professorship). D.P. thanks the University Grants Commission, Government of India, and JNCASR, India, for her Ph.D. fellowship. S.D. thanks the Department of Biotechnology, Government of India, for her postdoctoral fellowship. This work was financially supported by the Department of Biotechnology, Government of India (grant numbers BT/01/COE/07/09 and DBT/INF/22/SP27679/2018).

We declare that we have no competing interests.

Conceptualization: M.R.S.R., D.P. Methodology: D.P., S.D., D.P.I., D.S., M.R.S.R. Software: U.B. Validation: S.D., D.S. Formal Analysis: D.P., S.D., D.P.I., U.B. Investigation: D.P., S.D., D.P.I., U.B. Resources: M.R.S.R. Data curation: D.P., U.B. Writing - original draft and preparation: D.P., S.D. Writing - review and editing: M.R.S.R. Visualization: D.P., M.R.S.R. Supervision: M.R.S.R. Project administration: M.R.S.R. Funding acquisition: M.R.S.R.

REFERENCES

- Zhang P, Wu W, Chen Q, Chen M. 2019. Non-coding RNAs and their integrated networks. *J Integrative Bioinformatics* 16:20190027. <https://doi.org/10.1515/jib-2019-0027>.
- Marchese FP, Raimondi I, Huarte M. 2017. The multidimensional mechanisms of long noncoding RNA function. *Genome Biol* 18:206. <https://doi.org/10.1186/s13059-017-1348-2>.
- Jarroux J, Morillon A, Pinskaya M. 2017. History, discovery, and classification of lncRNAs. *Adv Exp Med Biol* 1008:1–46. https://doi.org/10.1007/978-981-10-5203-3_1.
- Hartford CCR, Lal A. 2020. When long noncoding becomes protein coding. *Mol Cell Biol* 40:e00528-19. <https://doi.org/10.1128/MCB.00528-19>.
- Xing J, Liu H, Jiang W, Wang L. 2020. lncRNA-encoded peptide: functions and predicting methods. *Front Oncol* 10:622294. <https://doi.org/10.3389/fonc.2020.622294>.
- Iyer MK, Niknafs YS, Malik R, Singhal U, Sahu A, Hosono Y, Barrette TR, Prensner JR, Evans JR, Zhao S, Poliakov A, Cao X, Dhanasekaran SM, Wu Y-M, Robinson DR, Beer DG, Feng FY, Iyer HK, Chinnaiyan AM. 2015. The landscape of long noncoding RNAs in the human transcriptome. *Nat Genet* 47:199–208. <https://doi.org/10.1038/ng.3192>.
- Kopp F, Mendell JT. 2018. Functional classification and experimental dissection of long noncoding RNAs. *Cell* 172:393–407. <https://doi.org/10.1016/j.cell.2018.01.011>.
- Wapinski O, Chang HY. 2011. Long noncoding RNAs and human disease. *Trends Cell Biol* 21:354–361. <https://doi.org/10.1016/j.tcb.2011.04.001>.
- Sun M, Kraus WL. 2015. From discovery to function: the expanding roles of long noncoding RNAs in physiology and disease. *Endocr Rev* 36:25–64. <https://doi.org/10.1210/er.2014-1034>.
- Li L, Zhuang Y, Zhao X, Li X. 2018. Long non-coding RNA in neuronal development and neurological disorders. *Front Genet* 9:744.
- Chen Y, Tergaonkar V. 2020. lncRNAs: master regulators in disease and cancer. *Proc Singapore Natl Acad Sci* 14:79–89. <https://doi.org/10.1142/S2591722620400062>.
- Rosa A, Ballarino M. 2016. Long noncoding RNA regulation of pluripotency. *Stem Cells Int* 2016:1797692. <https://doi.org/10.1155/2016/1797692>.
- Yoon JH, Abdelmohsen K, Gorospe M. 2013. Posttranscriptional gene regulation by long noncoding RNA. *J Mol Biol* 425:3723–3730. <https://doi.org/10.1016/j.jmb.2012.11.024>.
- Akhade VS, Pal D, Kanduri C. 2017. Long noncoding RNA: genome organization and mechanism of action. *Adv Exp Med Biol* 1008:47–74. https://doi.org/10.1007/978-981-10-5203-3_2.
- Zhao Y, Liu H, Zhang Q, Zhang Y. 2020. The functions of long non-coding RNAs in neural stem cell proliferation and differentiation. *Cell Biosci* 10:74. <https://doi.org/10.1186/s13578-020-00435-x>.
- Roberts TC, Morris KV, Wood MJ. 2014. The role of long non-coding RNAs in neurodevelopment, brain function and neurological disease. *Philos Trans R Soc B* 369:20130507. <https://doi.org/10.1098/rstb.2013.0507>.
- Briggs JA, Wolvetang EJ, Mattick JS, Rinn JL, Barry G. 2015. Mechanisms of long non-coding RNAs in mammalian nervous system development, plasticity, disease, and evolution. *Neuron* 88:861–877. <https://doi.org/10.1016/j.neuron.2015.09.045>.
- Hart RP, Goff LA. 2016. Long noncoding RNAs: central to nervous system development. *Int J Dev Neurosci* 55:109–116. <https://doi.org/10.1016/j.ijdevneu.2016.06.001>.
- Mercer TR, Dinger ME, Sunkin SM, Mehler MF, Mattick JS. 2008. Specific expression of long noncoding RNAs in the mouse brain. *Proc Natl Acad Sci U S A* 105:716–721. <https://doi.org/10.1073/pnas.0706729105>.
- Derrien T, Johnson R, Bussotti G, Tanzer A, Djebali S, Tilgner H, Guernec G, Martin D, Merkel A, Knowles DG, Lagarde J, Veeravalli L, Ruan X, Ruan Y,

- Lassmann T, Carninci P, Brown JB, Lipovich L, Gonzalez JM, Thomas M, Davis CA, Shiekhatter R, Gingers TR, Hubbard TJ, Notredame C, Harrow J, Guigó R. 2012. The GENCODE v7 catalog of human long noncoding RNAs: analysis of their gene structure, evolution, and expression. *Genome Res* 22:1775–1789. <https://doi.org/10.1101/gr.132159.111>.
21. Kadakkuzha BM, Liu XA, McCrate J, Shankar G, Rizzo V, Afinogenova A, Young B, Fallahi M, Carvalloza AC, Raveendra B, Puthanveetil SV. 2015. Transcriptome analyses of adult mouse brain reveal long enrichment of lncRNAs in specific brain regions and neuronal populations. *Front Cell Neurosci* 9:63.
 22. Liau WS, Samaddar S, Banerjee S, Bredy TW. 2021. On the functional relevance of spatiotemporally-specific patterns of experience-dependent long noncoding RNA expression in the brain. *RNA Biology* 18:1025–1036. <https://doi.org/10.1080/15476286.2020.1868165>.
 23. Lv J, Cui W, Liu H, He H, Xiu Y, Guo J, Liu H, Liu Q, Zeng T, Chen Y, Zhang Y, Wu Q. 2013. Identification and characterization of long non-coding RNAs related to mouse embryonic brain development from available transcriptomic data. *PLoS One* 8:e71152. <https://doi.org/10.1371/journal.pone.0071152>.
 24. Antoniou D, Stergiopoulos A, Politis PK. 2014. Recent advances in the involvement of long non-coding RNAs in neural stem cell biology and brain pathophysiology. *Front Physiol* 5:155.
 25. Dinger ME, Amaral PP, Mercer TR, Pang KC, Bruce SJ, Gardiner BB, Askarian-Amiri ME, Ru K, Soldà G, Simons C, Sunkin SM, Crowe ML, Grimmond SM, Perkins AC, Mattick JS. 2008. Long noncoding RNAs in mouse embryonic stem cell pluripotency and differentiation. *Genome Res* 18:1433–1445. <https://doi.org/10.1101/gr.078378.108>.
 26. Mohamed JS, Gaughwin PM, Lim B, Robson P, Lipovich L. 2010. Conserved long noncoding RNAs transcriptionally regulated by Oct4 and Nanog modulate pluripotency in mouse embryonic stem cells. *RNA* 16:324–337. <https://doi.org/10.1261/rna.1441510>.
 27. Hezroni H, Ben Tov Perry R, Gil N, Degani N, Ulitsky I. 2020. Regulation of neuronal commitment in mouse embryonic stem cells by the *Reno1/Bahcc1* locus. *EMBO Rep* 21:e51264.
 28. Goff LA, Groff AF, Sauvageau M, Traves-Gibson Z, Sanchez-Gomez DB, Morse M, Martin RD, Elcavage LE, Liapis SC, Gonzalez-Celeiro M, Plana O, Li E, Gerhardinger C, Tomassy GS, Arlotta P, Rinn JL. 2015. Spatiotemporal expression and transcriptional perturbations by long noncoding RNAs in the mouse brain. *Proc Natl Acad Sci U S A* 112:6855–6862. <https://doi.org/10.1073/pnas.1411263112>.
 29. Fullard JF, Hauberg ME, Bendt J, Egervari G, Cirnaru MD, Reach SM, Motl J, Ehrlich ME, Hurd YL, Roussos P. 2018. An atlas of chromatin accessibility in the adult human brain. *Genome Res* 28:1243–1252. <https://doi.org/10.1101/gr.232488.117>.
 30. Zhang L, Xue Z, Yan J, Wang J, Liu Q, Jiang H. 2019. lncRNA Riken-201 and Riken-203 modulates neural development by regulating the Sox6 through sequestering miRNAs. *Cell Prolif* 52:e12573. <https://doi.org/10.1111/cpr.12573>.
 31. Knauss JL, Miao N, Kim SN, Nie Y, Shi Y, Wu T, Pinto HB, Donohoe ME, Sun T. 2018. Long noncoding RNA Sox2ot and transcription factor YY1 co-regulate the differentiation of cortical neural progenitors by repressing Sox2. *Cell Death Dis* 9:799. <https://doi.org/10.1038/s41419-018-0840-2>.
 32. Ng SY, Bogu GK, Soh BS, Stanton LW. 2013. The long noncoding RNA RMST interacts with SOX2 to regulate neurogenesis. *Mol Cell* 51:349–359. <https://doi.org/10.1016/j.molcel.2013.07.017>.
 33. Nishant KT, Ravishankar H, Rao MRS. 2004. Characterization of a mouse recombination hot spot locus encoding a novel non-protein-coding RNA. *Mol Cell Biol* 24:5620–5634. <https://doi.org/10.1128/MCB.24.12.5620-5634.2004>.
 34. Ganesan G, Rao NM. 2008. A novel noncoding RNA processed by Drosha is restricted to nucleus in mouse. *RNA* 14:1399–1410. <https://doi.org/10.1261/rna.838308>.
 35. Arun G, Akhade VS, Donakonda S, Rao MRS. 2012. mrhl RNA, a long non-coding RNA, negatively regulates Wnt signaling through its protein partner Ddx5/p68 in mouse spermatogonial cells. *Mol Cell Biol* 32:3140–3152. <https://doi.org/10.1128/MCB.00006-12>.
 36. Akhade VS, Arun G, Donakonda S, Rao MRS. 2014. Genome wide chromatin occupancy of mrhl RNA and its role in gene regulation in mouse spermatogonial cells. *RNA Biol* 11:1262–1279. <https://doi.org/10.1080/15476286.2014.996070>.
 37. Akhade VS, Dighe SN, Kataruka S, Rao MRS. 2016. Mechanism of Wnt signaling induced down regulation of mrhl long non-coding RNA in mouse spermatogonial cells. *Nucleic Acids Res* 44:387–401. <https://doi.org/10.1093/nar/gkv1023>.
 38. Pal D, Neha CV, Bhaduri U, Zenia Z, Dutta S, Chidambaram S, Rao MRS. 2021. lncRNA Mrhl orchestrates differentiation programs in mouse embryonic stem cells through chromatin mediated regulation. *Stem Cell Res* 53:102250. <https://doi.org/10.1016/j.scr.2021.102250>.
 39. Fatima R, Choudhury SR, Divya TR, Bhaduri U, Rao MRS. 2019. A novel enhancer RNA, Hmrhl, positively regulates its host gene, phkb, in chronic myelogenous leukemia. *Noncoding RNA Res* 4:96–108. <https://doi.org/10.1016/j.ncrna.2019.08.001>.
 40. Choudhury SR, Dutta S, Bhaduri U, Rao MRS. 2021. lncRNA Hmrhl regulates expression of cancer related genes in chronic myelogenous leukemia through chromatin association. *NAR Cancer* 3:zcab042. <https://doi.org/10.1093/narcan/zcab042>.
 41. Yao B, Jin P. 2014. Unlocking epigenetic codes in neurogenesis. *Genes Dev* 28:1253–1271. <https://doi.org/10.1101/gad.241547.114>.
 42. Kirkeby A, Grealish S, Wolf DA, Nelander J, Wood J, Lundblad M, Lindvall O, Parmar M. 2012. Generation of regionally specified neural progenitors and functional neurons from human embryonic stem cells under defined conditions. *Cell Rep* 1:703–714. <https://doi.org/10.1016/j.celrep.2012.04.009>.
 43. Su Z, Zhang Y, Liao B, Zhong X, Chen X, Wang H, Guo Y, Shan Y, Wang L, Pan G. 2018. Antagonism between the transcription factors NANOG and OTX2 specifies rostral or caudal cell fate during neural patterning transition. *J Biol Chem* 293:4445–4455. <https://doi.org/10.1074/jbc.M117.815449>.
 44. Liu J, Wu X, Zhang H, Pfeifer GP, Lu Q. 2017. Dynamics of RNA polymerase II pausing and bivalent histone H3 methylation during neuronal differentiation in brain development. *Cell Rep* 20:1307–1318. <https://doi.org/10.1016/j.celrep.2017.07.046>.
 45. Bibel M, Richter J, Lacroix E, Barde YA. 2007. Generation of a defined and uniform population of CNS progenitors and neurons from mouse embryonic stem cells. *Nat Protoc* 2:1034–1043. <https://doi.org/10.1038/nprot.2007.147>.
 46. Plachta N, Bibel M, Tucker KL, Barde YA. 2004. Developmental potential of defined neural progenitors derived from mouse embryonic stem cells. *Development* 131:5449–5456. <https://doi.org/10.1242/dev.01420>.
 47. Castro DS, Martynoga B, Parras C, Ramesh V, Pacary E, Johnston C, Drechsel D, Lebel-Potter M, Garcia LG, Hunt C, Dolle D, Bithell A, Ettwiller L, Buckley N, Guillemot F. 2011. A novel function of the proneural factor *Ascl1* in progenitor proliferation identified by genome-wide characterization of its targets. *Genes Dev* 25:930–945. <https://doi.org/10.1101/gad.627811>.
 48. Bouchard M, Grote D, Craven SE, Sun Q, Steinlein P, Busslinger M. 2005. Identification of Pax2-regulated genes by expression profiling of the mid-hindbrain organizer region. *Development* 132:2633–2643. <https://doi.org/10.1242/dev.01833>.
 49. Wang H, Huo X, Yang X-R, He J, Cheng L, Wang N, Deng X, Jin H, Wang N, Wang C, Zhao F, Fang J, Yao M, Fan J, Qin W. 2017. STAT3-mediated up-regulation of lncRNA HOXD-AS1 as a ceRNA facilitates liver cancer metastasis by regulating SOX4. *Mol Cancer* 16:136. <https://doi.org/10.1186/s12943-017-0680-1>.
 50. Lee TY, Chang WC, Hsu JBK, Chang TH, Shien DM. 2012. GPMiner: an integrated system for mining combinatorial cis-regulatory elements in mammalian gene group. *BMC Genomics* 13:S3–12. <https://doi.org/10.1186/1471-2164-13-S1-S3>.
 51. Mathelier A, Zhao X, Zhang AW, Parcy F, Worsley-Hunt R, Arenillas DJ, Buchman S, Chen C-y, Chou A, Ienasescu H, Lim J, Shyr C, Tan G, Zhou M, Lenhard B, Sandelin A, Wasserman WW. 2014. JASPAR 2014: an extensively expanded and updated open-access database of transcription factor binding profiles. *Nucleic Acids Res* 42:D142–D147. <https://doi.org/10.1093/nar/gkt997>.
 52. Chenn A, Walsh CA. 2002. Regulation of cerebral cortical size by control of cell cycle exit in neural precursors. *Science* 297:365–369. <https://doi.org/10.1126/science.1074192>.
 53. Machon O, Van Den Bout CJ, Backman M, Kemler R, Krauss S. 2003. Role of β -catenin in the developing cortical and hippocampal neuroepithelium. *Neuroscience* 122:129–143. [https://doi.org/10.1016/S0306-4522\(03\)00519-0](https://doi.org/10.1016/S0306-4522(03)00519-0).
 54. Woodhead GJ, Mutch CA, Olson EC, Chenn A. 2006. Cell-autonomous β -catenin signaling regulates cortical precursor proliferation. *J Neurosci* 26:12620–12630. <https://doi.org/10.1523/JNEUROSCI.3180-06.2006>.
 55. Gaiano N, Nye JS, Fishell G. 2000. Radial glial identity is promoted by Notch1 signaling in the murine forebrain. *Neuron* 26:395–404. [https://doi.org/10.1016/S0896-6273\(00\)81172-1](https://doi.org/10.1016/S0896-6273(00)81172-1).
 56. Mizutani KI, Yoon K, Dang L, Tokunaga A, Gaiano N. 2007. Differential Notch signalling distinguishes neural stem cells from intermediate progenitors. *Nature* 449:351–355. <https://doi.org/10.1038/nature06090>.
 57. Imayoshi I, Sakamoto M, Yamaguchi M, Mori K, Kageyama R. 2010. Essential roles of Notch signaling in maintenance of neural stem cells in

- developing and adult brains. *J Neurosci* 30:3489–3498. <https://doi.org/10.1523/JNEUROSCI.4987-09.2010>.
58. Sakamoto M, Hirata H, Ohtsuka T, Bessho Y, Kageyama R. 2003. The basic helix-loop-helix genes *Hes1/Hey1* and *Hes2/Hey2* regulate maintenance of neural precursor cells in the brain. *J Biol Chem* 278:44808–44815. <https://doi.org/10.1074/jbc.M300448200>.
 59. Sansom SN, Griffiths DS, Faedo A, Kleinjan DJ, Ruan Y, Smith J, Van Heyningen V, Rubenstein JL, Livesey FJ. 2009. The level of the transcription factor *Pax6* is essential for controlling the balance between neural stem cell self-renewal and neurogenesis. *PLoS Genet* 5:e1000511. <https://doi.org/10.1371/journal.pgen.1000511>.
 60. Thakurela S, Tiwari N, Schick S, Garding A, Ivanek R, Berninger B, Tiwari VK. 2016. Mapping gene regulatory circuitry of *Pax6* during neurogenesis. *Cell Discov* 2:15045. <https://doi.org/10.1038/celldisc.2015.45>.
 61. Sun J, Rockowitz S, Xie Q, Ashery-Padan R, Zheng D, Cvekl A. 2015. Identification of in vivo DNA-binding mechanisms of *Pax6* and reconstruction of *Pax6*-dependent gene regulatory networks during forebrain and lens development. *Nucleic Acids Res* 43:6827–6846. <https://doi.org/10.1093/nar/gkv589>.
 62. Xie Q, Cvekl A. 2011. The orchestration of mammalian tissue morphogenesis through a series of coherent feed-forward loops. *J Biol Chem* 286:43259–43271. <https://doi.org/10.1074/jbc.M111.264580>.
 63. Xie Q, Yang Y, Huang J, Ninkovic J, Walcher T, Wolf L, Vitenzon A, Zheng D, Götz M, Beebe DC, Zavadii J, Cvekl A. 2013. *Pax6* interactions with chromatin and identification of its novel direct target genes in lens and forebrain. *PLoS One* 8:e54507. <https://doi.org/10.1371/journal.pone.0054507>.
 64. Pinson J, Mason JO, Simpson TI, Price DJ. 2005. Regulation of the *Pax6*: *Pax6* (5a) mRNA ratio in the developing mammalian brain. *BMC Dev Biol* 5:1–4. <https://doi.org/10.1186/1471-213X-5-13>.
 65. Kamachi Y, Uchikawa M, Tanouchi A, Sekido R, Kondoh H. 2001. *Pax6* and *SOX2* form a co-DNA-binding partner complex that regulates initiation of lens development. *Genes Dev* 15:1272–1286. <https://doi.org/10.1101/gad.887101>.
 66. Bouilloux F, Thireau J, Ventéo S, Farah C, Karam S, Dauvilliers Y, Valmier J, Copeland NG, Jenkins NA, Richard S, Marmigère F. 2016. Loss of the transcription factor *Meis1* prevents sympathetic neurons target-field innervation and increases susceptibility to sudden cardiac death. *Elife* 5:e11627. <https://doi.org/10.7554/eLife.11627>.
 67. Yamada T, Urano-Tashiro Y, Tanaka S, Akiyama H, Tashiro F. 2013. Involvement of crosstalk between *Oct4* and *Meis1a* in neural cell fate decision. *PLoS One* 8:e56997. <https://doi.org/10.1371/journal.pone.0056997>.
 68. Owa T, Taya S, Miyashita S, Yamashita M, Adachi T, Yamada K, Yokoyama M, Aida S, Nishioka T, Inoue YU, Goitsuka R, Nakamura T, Inoue T, Kaibuchi K, Hoshino M. 2018. *Meis1* coordinates cerebellar granule cell development by regulating *Pax6* transcription, BMP signaling and *Atoh1* degradation. *J Neurosci* 38:1277–1294. <https://doi.org/10.1523/JNEUROSCI.1545-17.2017>.
 69. Vihma H, Luhakooder M, Pruunsild P, Timmusk T. 2016. Regulation of different human NFAT isoforms by neuronal activity. *J Neurochem* 137:394–408. <https://doi.org/10.1111/jnc.13568>.
 70. Wild AR, Sinnen BL, Dittmer PJ, Kennedy MJ, Sather WA, Dell'Acqua ML. 2019. Synapse-to-nucleus communication through NFAT is mediated by L-type Ca^{2+} channel Ca^{2+} spike propagation to the soma. *Cell Rep* 26:3537–3550.E4. <https://doi.org/10.1016/j.celrep.2019.03.005>.
 71. Chalei V, Sansom SN, Kong L, Lee S, Montiel JF, Vance KW, Ponting CP. 2014. The long non-coding RNA *Dali* is an epigenetic regulator of neural differentiation. *Elife* 3:e04530. <https://doi.org/10.7554/eLife.04530>.
 72. Xu Y, Xi J, Wang G, Guo Z, Sun Q, Lu C, Ma L, Wu Y, Jia W, Zhu S, Guo X, Bian S, Kang J. 2021. PAUPAR and PAX6 sequentially regulate human embryonic stem cell cortical differentiation. *Nucleic Acids Res* 49:1935–1950. <https://doi.org/10.1093/nar/gkab030>.
 73. Alammari F. 2019. KAP1-Paupar lncRNA chromatin regulatory complex controls subventricular zone neurogenesis. PhD thesis, University of Oxford, Oxford, United Kingdom.
 74. Feng J, Bi C, Clark BS, Mady R, Shah P, Kohtz JD. 2006. The *Evf-2* noncoding RNA is transcribed from the *Dlx-5/6* ultraconserved region and functions as a *Dlx-2* transcriptional coactivator. *Genes Dev* 20:1470–1484. <https://doi.org/10.1101/gad.1416106>.
 75. Stamou M, Ng S-Y, Brand H, Wang H, Plummer L, Best L, Havlicek S, Hibberd M, Khor CC, Gusella J, Balasubramanian R, Talkowski M, Stanton LW, Crowley WF. 2020. A balanced translocation in Kallmann syndrome implicates a long noncoding RNA, *RMST*, as a GnRH neuronal regulator. *J Clin Endocrinol Metab* 105:e231–e244. <https://doi.org/10.1210/clinem/dgz011>.
 76. Andersen RE. 2019. The novel long noncoding RNA *Pnky* regulates neurogenesis and neural stem cell maintenance in vivo. PhD thesis, University of California, San Francisco, CA.
 77. Ramos AD, Andersen RE, Liu SJ, Nowakowski TJ, Hong SJ, Gertz CC, Salinas RD, Zarabi H, Kriegstein AR, Lim DA. 2015. The long noncoding RNA *Pnky* regulates neuronal differentiation of embryonic and postnatal neural stem cells. *Cell Stem Cell* 16:439–447. <https://doi.org/10.1016/j.stem.2015.02.007>.
 78. Tian K, Wang A, Wang J, Li W, Shen W, Li Y, Luo Z, Liu Y, Zhou Y. 2021. Transcriptome analysis identifies *SenZfp536*, a sense lncRNA that suppresses self-renewal of cortical neural progenitors. *Neurosci Bull* 37:183–200. <https://doi.org/10.1007/s12264-020-00607-2>.
 79. Cui Y, Yin Y, Xiao Z, Zhao Y, Chen B, Yang B, Xu B, Song H, Zou Y, Ma X, Dai J. 2019. lncRNA *Neat1* mediates miR-124-induced activation of *Wnt/β-catenin* signaling in spinal cord neural progenitor cells. *Stem Cell Res Ther* 10:400. <https://doi.org/10.1186/s13287-019-1487-3>.
 80. Zhang L, Yan J, Liu Q, Xie Z, Jiang H. 2019. lncRNA *Rik-203* contributes to anesthesia neurotoxicity via microRNA-101a-3p and GSK-3β-mediated neural differentiation. *Sci Rep* 9:6822. <https://doi.org/10.1038/s41598-019-42991-4>.
 81. Wu SC, Kallin EM, Zhang Y. 2010. Role of H3K27 methylation in the regulation of lncRNA expression. *Cell Res* 20:1109–1116. <https://doi.org/10.1038/cr.2010.114>.
 82. Wu Z, Liu X, Liu L, Deng H, Zhang J, Xu Q, Cen B, Ji A. 2014. Regulation of lncRNA expression. *Cell Mol Biol Lett* 19:561–575. <https://doi.org/10.2478/s11658-014-0212-6>.
 83. Engreitz JM, Haines JE, Perez EM, Munson G, Chen J, Kane M, McDonel PE, Guttman M, Lander ES. 2016. Local regulation of gene expression by lncRNA promoters, transcription and splicing. *Nature* 539:452–455. <https://doi.org/10.1038/nature20149>.
 84. Zelinger L, Karakulah G, Chaitankar V, Kim JW, Yang HJ, Brooks MJ, Swaroop A. 2017. Regulation of noncoding transcriptome in developing photoreceptors by rod differentiation factor *NRL*. *Invest Ophthalmol Vis Sci* 58:4422–4435. <https://doi.org/10.1167/iovs.17-21805>.
 85. Sun Z, Huang G, Cheng H. 2019. Transcription factor *Nrf2* induces the up-regulation of lncRNA *TUG1* to promote progression and adriamycin resistance in urothelial carcinoma of the bladder. *Cancer Manag Res* 11:6079–6090. <https://doi.org/10.2147/CMAR.S200998>.
 86. Huang T, Wang G, Yang L, Peng B, Wen Y, Ding G, Wang Z. 2017. Transcription factor *YY1* modulates lung cancer progression by activating lncRNA-PVT1. *DNA Cell Biol* 36:947–958. <https://doi.org/10.1089/dna.2017.3857>.
 87. Sun J, Zhao Y, McGreal R, Cohen-Tayar Y, Rockowitz S, Wilczek C, Ashery-Padan R, Shechter D, Zheng D, Cvekl A. 2016. *Pax6* associates with H3K4-specific histone methyltransferases *Mll1*, *Mll2*, and *Set1a* and regulates H3K4 methylation at promoters and enhancers. *Epigenet Chromatin* 9:37. <https://doi.org/10.1186/s13072-016-0087-z>.
 88. Pijnappel WP, Baltissen MP, Timmers HM. 2013. Protocol for lentiviral knock down in mouse ES cells. *Protocol Exchange*. <https://doi.org/10.1038/protex.2013.036>.
 89. de Planell-Saguer M, Rodicio MC, Mourelatos Z. 2010. Rapid in situ codection of noncoding RNAs and proteins in cells and formalin-fixed paraffin-embedded tissue sections without protease treatment. *Nat Protoc* 5:1061–1073. <https://doi.org/10.1038/nprot.2010.62>.
 90. Cotney JL, Noonan JP. 2015. Chromatin immunoprecipitation with fixed animal tissues and preparation for high-throughput sequencing. *Cold Spring Harb Protoc* 2015:191–199. <https://doi.org/10.1101/pdb.prot084848>.
 91. Furlan-Magaril M, Rincón-Arango H, Recillas-Targa F. 2009. Sequential chromatin immunoprecipitation protocol: ChIP-reChIP. *Methods Mol Biol* 543:253–266. https://doi.org/10.1007/978-1-60327-015-1_17.
 92. Uchil PD, Nagarajan A, Kumar P. 2017. Assay for β-galactosidase in extracts of mammalian cells. *Cold Spring Harb Protoc* 2017:pdb.prot095778. <https://doi.org/10.1101/pdb.prot095778>.
 93. Grant CE, Bailey TL, Noble WS. 2011. FIMO: scanning for occurrences of a given motif. *Bioinformatics* 27:1017–1018.